

Alma Mater Studiorum Università di Bologna
Archivio istituzionale della ricerca

(±)- BIGI-3h: Pentatarget-Directed Ligand combining Cholinesterase, Monoamine Oxidase, and Glycogen Synthase Kinase 3 β Inhibition with Calcium Channel Antagonism and Antiaggregating Properties for Alzheimer's Disease

This is the final peer-reviewed author's accepted manuscript (postprint) of the following publication:

Published Version:

Ismaili L., Monnin J., Etievant A., Arribas R.L., Viejo L., Refouvelet B., et al. (2021). (±)- BIGI-3h: Pentatarget-Directed Ligand combining Cholinesterase, Monoamine Oxidase, and Glycogen Synthase Kinase 3 β Inhibition with Calcium Channel Antagonism and Antiaggregating Properties for Alzheimer's Disease. ACS CHEMICAL NEUROSCIENCE, 12(8), 1328-1342 [10.1021/acscchemneuro.0c00803].

Availability:

This version is available at: <https://hdl.handle.net/11585/855822> since: 2024-11-13

Published:

DOI: <http://doi.org/10.1021/acscchemneuro.0c00803>

Terms of use:

Some rights reserved. The terms and conditions for the reuse of this version of the manuscript are specified in the publishing policy. For all terms of use and more information see the publisher's website.

This item was downloaded from IRIS Università di Bologna (<https://cris.unibo.it/>).
When citing, please refer to the published version.

(Article begins on next page)

(±)-BIGI-3h: Pentatarget-Directed Ligand combining Cholinesterase, Monoamine Oxidase and Glycogen Synthase Kinase 3 β Inhibition with Calcium Channel Antagonism and antiaggregating properties for Alzheimer's Disease

Lhassane Ismaili*¹, Julie Monnin¹, Adeline Etievant¹, Raquel L. Arribas², Lucía Viejo², Bernard Refouvelet¹, Ondrej Soukup³, Jana Janockova³, Vendula Hepnarova⁴, Jan Korabecny³, Tomas Kucera⁴, Daniel Jun⁴, Rudolf Andrys⁵, Kamil Musilek⁵, Aurelie Baguet⁶, Eva M García-Frutos⁷, Angela De Simone⁸, Vincenza Andrisano⁸, Manuela Bartolini⁹, Cristóbal de los Ríos², José Marco-Contelles¹⁰ and Emmanuel Haffen¹.

¹Neurosciences intégratives et cliniques EA 481, Univ. Bourgogne Franche-Comté, F-25000 Besançon, France.

²Servicio de Farmacología Clínica, Instituto de Investigación Sanitaria, Hospital Universitario de la Princesa, C/ Diego de León, 62, 28006 Madrid (Spain) and Instituto Teofilo Hernando, Universidad Autónoma de Madrid, C/ Arzobispo Morcillo, 4, 28029 Madrid (Spain)

³Biomedical Research Center, University Hospital Hradec Kralove, Czech Republic, University of Defence, Hradec Kralove, (Czech Republic)

⁴Department of Toxicology and Military Pharmacy, Faculty of Military Health Sciences (Czech Republic)

⁵University Hradec Kralove, Faculty of Science, Department of Chemistry, Rokitanskeho 62, 50003 Hradec Kralove, (Czech Republic)

⁶Université Bourgogne Franche Comté, France, INSERM, UMR1098, Interactions Hôte-Greffon-Tumeur/Ingénierie Cellulaire et Génique, F-25000, Besançon, (France).

⁷Instituto de Ciencia de Materiales de Madrid, CSIC, Cantoblanco 28049, Madrid (Spain)

⁸Department for Life Quality Studies University of Bologna Corso di Augusto, 237, 47921-Rimini, (Italy)

⁹Department of Pharmacy and Biotechnology Alma Mater Studiorum—University of Bologna Via Belmeloro 6, 40126-Bologna, (Italy)

¹⁰Laboratory of Medicinal Chemistry (Instituto de Química Orgánica General, Consejo Superior de Investigaciones Científicas), Juan de la Cierva 3; 28006-Madrid, Spain

Abstract

Multitarget-directed ligands (MTDLs) are considered a promising therapeutic strategy to address the multifactorial nature of Alzheimer's disease (AD). Novel MTDLs have been designed as inhibitors of human acetyl-/butyrylcholinesterases, monoamine oxidase A/B, glycogen synthase kinase 3 β and as calcium channel antagonists via the Biginelli multicomponent reaction. Among these MTDLs, **(±)-BIGI-3h** was identified as a promising new hit compound showing *in vitro* balanced activities toward the aforementioned recognized AD targets. Additional *in vitro* studies demonstrated antioxidant effects and brain penetration, along with the ability to inhibit the aggregation of both tau protein and beta-amyloid peptide. *In vivo* studies have shown that **(±)-BIGI-3h** (10 mg/kg intraperitoneally) significantly reduces scopolamine-induced cognitive deficits.

Keywords

Alzheimer's disease, Calcium Channel, GSK 3 β , MAO, Cholinesterase, Biginelli reaction

INTRODUCTION

Alzheimer's Disease (AD) is now considered an extensively complex and multifactorial neurodegenerative disorder with no available cure till the moment. Despite unprecedented amounts of scientific publications (more than 100K in Pubmed), current offered treatments are limited to a temporary relief of symptoms¹. AD is the most common cause of memory impairment and dementia in elderly people². It is characterized by a series of highly interconnected pathological processes that are hallmarked by (i) the accumulation of abnormal levels of soluble aggregates and extracellular deposits of amyloid-beta peptide (A β) and (ii) the formation of neurofibrillary tangles, which are composed of hyperphosphorylated tau protein³.

The formation of A β deposits in the brain is a critical step and it was associated with the progression and development of AD. It is indeed now widely accepted that A β toxicity is mainly related to A β prefibrillar and brain permeable species since A β oligomers have been shown to accelerate neuronal cell death and to adversely affect synaptic function⁴.

Hyperphosphorylation renders tau prone to aggregate and to impair cell viability⁵. This aggregation, once initiated, is self-replicating, depleting the physiological tau pool in the neuron and converting it to toxic neurofibrillary tangles which continue to accumulate, leading to neuronal toxicity⁶.

These pathological structures ultimately lead to a progressive loss of cholinergic neurons, memory impairment, and cognitive dysfunction⁷.

The disease is also characterized by low levels of acetylcholine, which is enhanced by the administration of cholinesterase (ChE) inhibitors, one of the primary therapeutic options available⁸.

Regarding mechanisms underlying neurodegeneration, the increase in cytosolic calcium levels has been identified as a crucial factor. Indeed, increased levels of calcium have been shown to facilitate the formation of A β by increasing the activity of β -secretase^{9,10} and regulating glycogen synthase kinase 3 (GSK-3 β)¹¹. In addition, the entry of calcium through L-type voltage-gated calcium channels (VGCC) results in calcium overload, mitochondrial disruption, and cell apoptosis activation¹².

Furthermore, GSK-3 β , which is a major kinase involved in the phosphorylation of tau, has been implicated in AD and AD-related tau pathology^{13,14}, has an important role in other AD key features such

as inflammation and apoptosis and its levels have been shown to be abnormally increased in the brain of patients with AD¹⁵.

Other significant factors such oxidative stress (OS) has been identified as crucial elements in AD pathogenesis. OS is caused by various underlying factors such as mitochondrial dysfunction¹⁶, disturbance in the homeostasis of biometals (Cu, Fe, Zn) linked to their involvement in peptide A β aggregation¹⁷, neuroinflammation¹⁸, or hydrogen peroxide (H₂O₂) production in the MAO-catalyzed deamination reaction of biogenic amines¹⁹. In fact, it is well known that MAO-B plays a pivotal role in the progression of AD²⁰, and its expression in neuronal tissues increases with aging, resulting in increased dopamine metabolism and higher levels of hydrogen peroxide that can cause further oxidative free radicals.

Given the above-mentioned evidence, the development of multitarget directed ligands (MTDLs), i.e., small molecules able to hit multiple targets responsible for AD pathogenesis, has been pursued, in recent years, as innovative AD medications and therapeutic opportunity to face to this complex scenario. Several MTDLs were developed with promising profiles, however, none hasn't been approved so far for the treatment of AD²¹⁻²⁴.

Multicomponent reactions (MCRs) are atom economic where most atoms of starting materials, if not all, are found in the product. Thus, MCRs are a useful alternative to sequential multistep syntheses, allowing scaffold diversity and a rapid and easy access to biologically relevant compounds^{25,26}. Therefore, MCRs seem well-suited for the search of new MTDL able to simultaneously interact with various biological targets concerning AD²⁷.

In previous works, we have developed a number of new MTDL using MCR such Ugi and Hantzsch^{24,27-30}. Herein, we report the design, synthesis, via Biginelli MCR, and biological evaluation of new family of **BIGI-3a-n** named ethyl 1-(2-(1-benzylpiperidin-4-yl)ethyl)-6-methyl-2-oxo-4-(4-oxo-4H-chromen-3-yl)-1,2,3,4-tetrahydropyrimidine-5-carboxylate (Figure 1). These compounds possess a selected benzylpiperidine motif of donepezil and chromone. Donepezil is an anti-AD drug that acts as a selective AChE inhibitor, and chromone is a privileged scaffold in medicinal chemistry, exhibiting a wide range of pharmacological activities such as antioxidant properties and inhibitory activities against both MAO and A β self-aggregation³¹. The Biginelli one-pot reaction, one of the very known

multicomponent reaction, was used not only for its interest as MCR but also to generate the central dihydropyridinone core, which has a potential calcium channel modulation activity similar to classical dihydropyridines³², such as **SQ32926**^{32,33}. (Figure 1). This scaffold might also modulate GSK-3 β , as it has the cyclic urea group present in several GSK-3 β inhibitors such as phenylmethylenhydantoin¹⁵, **SB-415286**³⁴, or the triazinones reported by Prati et al³⁵.

From these studies, we have identified **BIGI-3h**, the first small-molecule MTDL that can simultaneously modulate ChEs, GSK3 β , and monoamine oxidase (MAO); counteract calcium overload through the inhibition of VGCC; exert antioxidant activity; and inhibit A β and Tau aggregation. This multitarget profile might contribute to an original and innovative therapeutic approach for the effective treatment of AD.

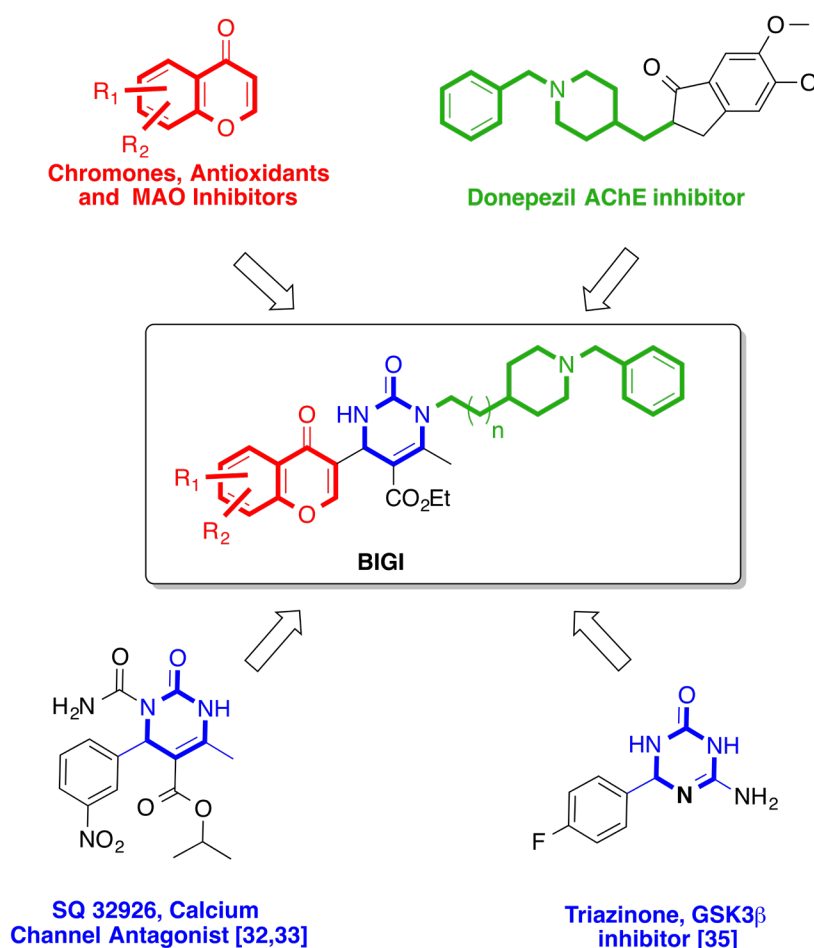


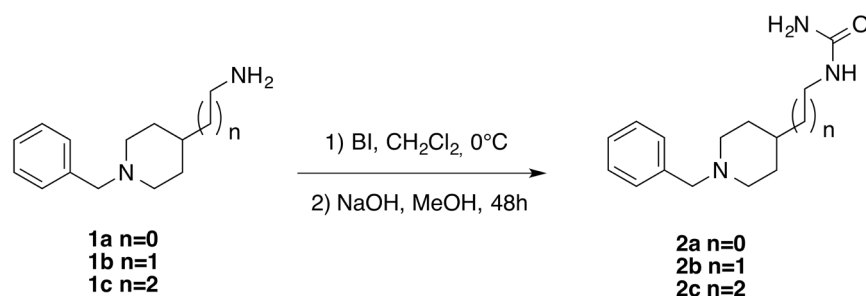
Figure 1. Design of **BIGI** compounds with potential inhibitory activity against cholinesterase (ChE), MAO, and GSK-3 β and with calcium channel blockade activity

RESULTS AND DISCUSSION

Chemistry

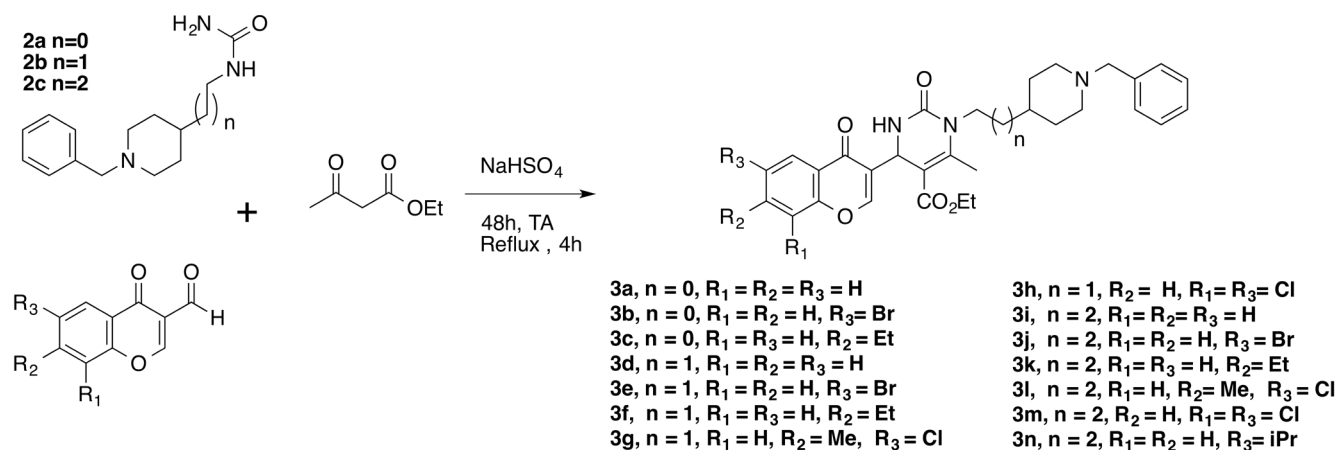
The syntheses of the **BIGI** compounds **3a-n** (Scheme 2) have been carried out using new one-pot Biginelli reaction conditions of compounds **2a-c**, ethyl acetoacetate, different commercial 3-formyl chromones and sodium bisulfate as a catalyst in acetic acid at room temperature for 60 h and refluxed for additional 4h. Compounds **2a-c** were obtained from commercial benzylpiperidines **1a-b** ($n=0,1$) or **1c**³⁶ ($n=2$) with the benzoyl isocyanate (BI), in CH_2Cl_2 at 0°C for 1 hour, followed by hydrolysis of the resulting compounds with NaOH for 48 hours³⁷ (scheme 1). All new compounds were characterized using analytical (HPLC) and spectroscopic data (^1H and ^{13}C NMR, ESI-MS or elemental analysis) showing data in good agreement with their structure which are collected in the Experimental Section and Supporting Information

Scheme 1: Synthetic procedure for the Synthesis of ureas **2a-c**



BI = Benzoyl isocyanate

Scheme 2. Synthesis of **BIGI-3a-n** using *one-pot* Biginelli reaction.



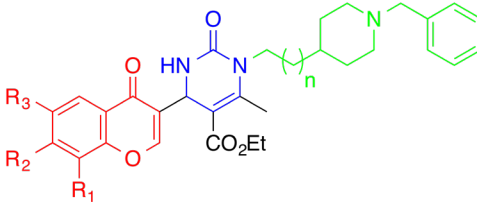
Biological evaluation

To verify the effectiveness of our compounds to simultaneously hit the selected targets and to make a judicious use of resources, blockade of VGCC and inhibition of human ChE (hChE), which are rational targets for **BIGIs**, as well as antioxidant activity were selected as the first filters for the selection of the promising compounds. Then, the latter were evaluated as A β aggregation inhibitors and for their abilities to cross the blood-brain barrier (BBB) leading to a promising hit compound for AD treatment which was further investigated as MAO, GSK3 β and Tau aggregation inhibitor.

Calcium channel antagonism. We investigated the blocking effect of the depolarization-induced Ca²⁺ uptake in SH-SY5Y neuroblastoma cells stimulated with an extracellular concentration of K⁺ 70 mM, which induces the cell Ca²⁺ levels elevation by opening voltage-gated Ca²⁺ channels (VGCC), monitored with the Ca²⁺-sensitive fluorescent dye Fluo-4. The results are listed in Table 1 showing among the 14 **BIGIs** assessed, 11 displayed better VGCC inhibitory activity than nifedipine, which is a calcium channel blocker medication used as positive standard, with IC₅₀ ranging from 1.4 to 6 μ M. The three compounds that possessed an IC₅₀ higher than nifedipine lacked substitution on the chromone moiety, regardless of the length of the linker (Table 1).

Inhibition of human AChE/human BuChE. Cholinesterase inhibition of compounds **BIGI-3a-n** was evaluated following the Ellman protocol³⁸. As shown in Table 1, the synthesized **BIGIs** generally exhibited good inhibition against human acetylcholinesterase (hAChE) in the submicromolar range and against human butyrylcholinesterase (hBuChE) in the micromolar range, thus behaving as selective AChEI. Particularly, compounds **BIGI-3e** and **BIGI-3h**, with a linker length of n=1, had an IC₅₀ of 0.06 μ M for hAChE and therefore only 3-fold less actives than Donepezil with IC₅₀ of 0.02 μ M, while the most potent inhibitor of hBuChE was **BIGI-3k** (IC₅₀ = 2.95 μ M). It is worth noting that, **BIGI-3e**, **BIGI-3h** and **BIGI-3k** were also the best VGCC blockers

Concerning structure activity relationship, a linker length of n=0 seemed detrimental for AChE inhibitory activity. Except for compound **BIGI-3a**, all compounds showed the same trend for hBuChE inhibition. For the same linker length (n=1 or 2), the best results were obtained with a chromone bearing an ethyl group (R₂ = Et) or having no substituents.

Table 1: Calcium channel blockade, hChE inhibition, and ORAC analysis of **BIGI-3a-n** and reference compounds^a


3a, n = 0, R₁ = R₂ = R₃ = H
3b, n = 0, R₁ = R₂ = H, R₃ = Br
3c, n = 0, R₁ = R₃ = H, R₂ = Et
3d, n = 1, R₁ = R₂ = R₃ = H
3e, n = 1, R₁ = R₂ = H, R₃ = Br
3f, n = 1, R₁ = R₃ = H, R₂ = Et
3g, n = 1, R₁ = H, R₂ = Me, R₃ = Cl
3h, n = 1, R₂ = H, R₁ = R₃ = Cl
3i, n = 2, R₁ = R₂ = R₃ = H
3j, n = 2, R₁ = R₂ = H, R₃ = Br
3k, n = 2, R₁ = R₃ = H, R₂ = Et
3l, n = 2, R₁ = H, R₂ = Me, R₃ = Cl
3m, n = 2, R₂ = H, R₁ = R₃ = Cl
3n, n = 2, R₁ = R₂ = H, R₃ = iPr

Compounds	Calcium channel blockade IC ₅₀ (μM)	hAChE inhibition (IC ₅₀ μM)	hBuChE inhibition (IC ₅₀ μM)	ORAC ^c
BIGI-3a	14 ± 3	n.a.	14.8 ± 0.7	3.29 ± 0.07
BIGI-3b	6 ± 3	n.a.	n.a.	2.06 ± 0.17
BIGI-3c	3.0 ± 0.9	6.08 ± 0.38	36.1 ± 3.1	3.51 ± 0.09
BIGI-3d	9 ± 2	0.23 ± 0.01	6.58 ± 0.34	2.53 ± 0.17
BIGI-3e	1.9 ± 0.6	0.06 ± 0.00	8.4 ± 0.34	3.26 ± 0.12
BIGI-3f	2.2 ± 0.6	0.30 ± 0.01	5.96 ± 0.22	2.20 ± 0.05
BIGI-3g	1.7 ± 0.6	0.29 ± 0.01	15.7 ± 0.9	2.56 ± 0.13
BIGI-3h	1.4 ± 0.4	0.06 ± 0.00	17.3 ± 0.9	3.65 ± 0.07
BIGI-3i	8 ± 1	0.15 ± 0.00	4.29 ± 0.09	3.09 ± 0.07
BIGI-3j	3.8 ± 0.1	0.18 ± 0.01	6.51 ± 0.45	3.24 ± 0.02
BIGI-3k	1.4 ± 0.5	0.50 ± 0.02	2.95 ± 0.14	2.75 ± 0.16
BIGI-3l	3.2 ± 0.2	0.17 ± 0.01	6.26 ± 0.31	1.68 ± 0.18
BIGI-3m	5 ± 2	0.34 ± 0.02	14.4 ± 1.2	3.29 ± 0.10
BIGI-3n	1.7 ± 0.4	0.58 ± 0.02	4.35 ± 0.23	2.45 ± 0.04
Nifedipine	6.2 ± 0.2	^b	^b	^b
Donepezil ³⁹	^b	0.02 ± 0.01	7.4 ± 0.39	^b
Tacrine ⁴⁰	^b	1.33 ± 0.04	0.049 ± 0.002	^b
Melatonin	^b	^b	^b	2.5 ± 0.1
Ferulic acid	^b	^b	^b	3.7 ± 0.2

^aEach IC₅₀ is the mean ± standard error of mean of at least three different experiments performed in quadruplicate; ^bnot evaluated, n.a.: not active, % inhibition under 50%. ^cData are expressed as micromoles of trolox equivalents/μmol tested compound and are shown as means ± standard error of means.

Antioxidant activity. The capacity of **BIGI-3a-n** to reduce the amount of peroxy radicals was determined by the Oxygen Radical Absorbance Capacity by Fluorescence (ORAC-FL) method,^{41,42} using Trolox as standard compound and fluorescein (FL) as the fluorescent probe. The results were expressed as Trolox equivalents (μmol of trolox/μmol of tested compound, TE). All compounds exhibited strong antioxidant activity with Trolox equivalent values ranging from 1.68 TE (**BIGI-3l**) to 3.65 TE (**BIGI-3h**), similar to that of standards such as melatonin (2.5 TE) and ferulic acid (3.7 TE). Interestingly **BIGI-3h** was the most active compounds while, **BIGI-3e** and **BIGI-3k** showed respectively 3.26 TE and 2.75 TE

Interestingly, the most balanced compounds considering VGCC and hChE inhibition showed also strong antioxidant activity; **BIGI-3h** was the most active compounds while, **BIGI-3e** and **BIGI-3k** showed respectively 3.26 TE and 2.75 TE. Therefore, we examined whether these selected **BIGI** compounds inhibited Aβ aggregation³¹ and crossed the blood-brain barrier (BBB).

Inhibition of A β ₁₋₄₂ aggregation. The inhibitory activity of selected **BIGI-3e**, **BIGI-3h**, and **BIGI-3k** against spontaneous aggregation of A β ₁₋₄₂ was determined *in vitro* using a thioflavin T-based fluorometric assay⁴³. Curcumin was used as positive control while tacrine, the first approved anti-AD drug was used as negative control. The three **BIGI** compounds, screened at 50 μ M concentration, showed good A β ₁₋₄₂ anti-aggregation activity (Table 2), with inhibition percentages in the narrow range of 63–66% when tested at equimolar concentrations with A β ₁₋₄₂. Their inhibitory potencies were only slightly lower than that of curcumin, a well-known anti-aggregating agent against amyloid peptides, tested under the same experimental conditions.

Table 2. Efficacy of BIGI-3e , 3k , and 3h to inhibit A β ₁₋₄₂ aggregation and their ability to cross blood-brain barrier. Curcumin and tacrine were used as positive and negative reference compounds, respectively.		
Compounds	% Inhibition A β ₁₋₄₂ aggregation ^a	CNS
BIGI-3e	63.0 \pm 2.1	CNS (+/-)
BIGI-3k	63.8 \pm 0.8	CNS (-)
BIGI-3h	66.0 \pm 0.7	CNS (+)
Tacrine	6.3 \pm 2.1	CNS (+)
Curcumin	74.5 \pm 0.5	n.d.

^a % inhibition of A β ₁₋₄₂ aggregation by the tested compounds. [A β] = [Inhibitor] = 50 μ M. Data are the means \pm standard error of means of two experiments each performed in duplicate. n.d., Not determined. CNS, central nervous system.

In vitro Blood–Brain Barrier Permeability. A major problem to overcome in CNS drug discovery is the ability of the compound in question to cross the BBB at therapeutic concentrations. Therefore the three compounds were evaluated using Parallel artificial membrane permeability assay (PAMPA)⁴⁴ which is a high throughput technique developed to predict BBB passive permeability. Despite all three compounds having similar activity profiles, only compound **BIGI-3h** could cross the BBB via passive diffusion (Table 2). Consequently, **BIGI-3h** was selected as a promising hit compound for AD treatment and was further investigated.

IN-DEPTH EXPLORATION OF **BIGI-3h**

Firstly, as **BIGI-3h** contains a stereocenter and chirality may play a role in the biological activity toward selected targets, its enantiomers were separated by chiral high-performance liquid chromatography, and each enantiomerically pure forms were evaluated as Calcium channel antagonists, ChE and A β

inhibitors. (\pm)-**BIGI-3h**, (+)-**BIGI-3h**, and (-)-**BIGI-3h** were also evaluated to assess their inhibitory activity toward MAO and GSK-3 β , as well as against Tau (306-336) aggregation.

Results showed only slight activity variations in these pure compounds compared to the racemate **BIGI-3h** (Table 3), regarding, the inhibition of hAChE (as confirmed by molecular modeling, **see below**), the blockade of VGCC, and the aggregation of A β as well as their ability to cross the BBB.

In silico modelling of the two enantiomers of BIGI-3h. To disclose the proposed dual binding mode and to assign the structural requirements determining the affinities of each enantiomer, we have performed molecular modeling studies for (*R*)-**BIGI-3h** and (*S*)-**BIGI-3h** in hAChE active site obtained from RCSB Protein Data Bank (PDB ID: 4EY7; Figure 2). The validity of our study is further corroborated by the fact that the enzyme of the same origin was used for *in vitro* evaluation.⁴⁵ Moreover, the consistency is also supported by the resemblance of **BIGI-3h** to donepezil by possessing *N*-benzylpiperidine fragment.

Indeed, both enantiomers share high degree of homology in their lodging and affinity to hAChE as predicted by our experimental protocol exploiting AutoDock Tools.⁴⁶⁻⁴⁹ (*R*)-**BIGI-3h** (Figure 2 A, B) revealed dual binding site pattern with *N*-benzylpiperidine being oriented outwards the cavity gorge, while 6,8-dichloro-4*H*-chromen-4-one was placed centrally. This is somewhat contradictory to donepezil-hAChE anchoring in crystal structure since *N*-benzylpiperidine was found to be stacked against Trp86 in the catalytic anionic site (CAS; Figure 3).^{45,50} More in detail, *N*-benzyl ring of (*R*)-**BIGI-3h** is stacked against Trp286 (4.1 Å), key amino acid residue of hAChE peripheral anionic site (PAS).⁵¹ Additionally, the ligand is also engaged in cation- π interaction between nitrogen of piperidine and Trp286 (4.6 Å). In the mid-gorge AChE region, the ligand is implicated in several π -alkyl interactions between Tyr124, Phe338 and Phe297 and methyl together with ethyl-carboxylate appendages of ethyl 6-methyl-2-oxo-1,2,3,4-tetrahydropyrimidine-5-carboxylate moiety. At the bottom of the gorge, 6,8-dichloro-4*H*-chromen-4-one displayed putative face-to-face π - π interaction with Trp86 (3.6 Å) and displaced π - π interaction with Tyr337 (3.4 Å). Hydrogen situated at the nitrogen from heterocyclic indole of Trp86 (2.2 Å) formed favorable hydrogen contact to carbonyl from ethyl-carboxylate appendage. Ser203 as well His447 from catalytic triad showed van der Waals contacts with ligand further improving ligand stabilization.

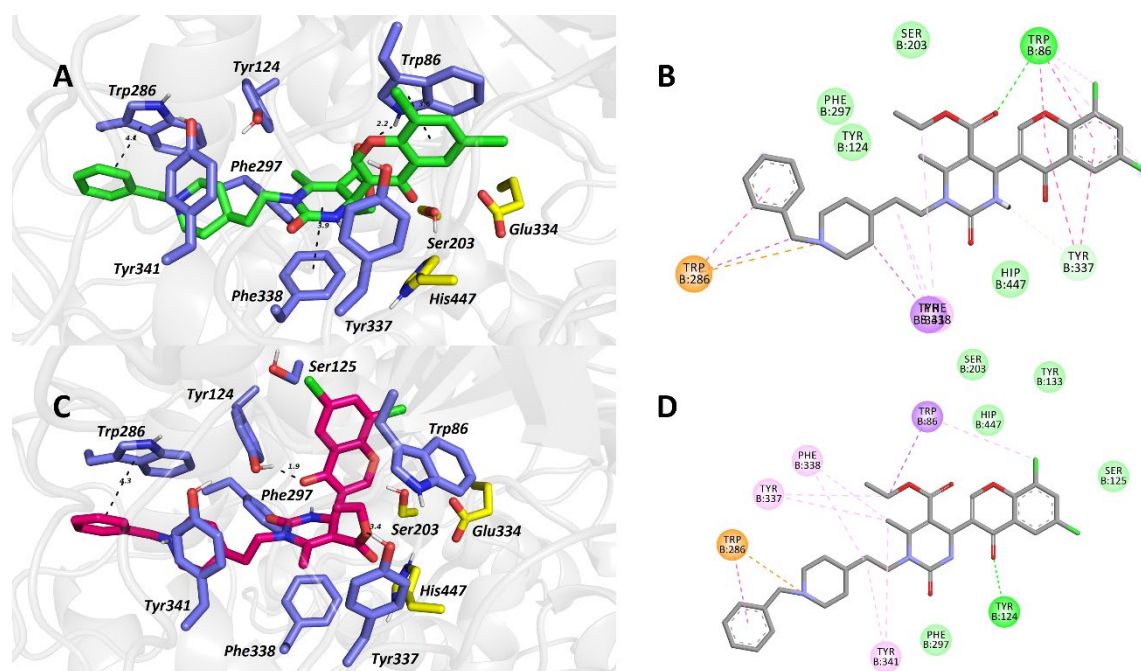


Figure 2. Top-scored docking poses of (*R*)-**BIGI-3h** (A, B) and (*S*)-**BIGI-3h** (C, D) complexed with *hAChE* (PDB ID: 4EY7). Generally to A and C—(*R*)-**BIGI-3h** and (*S*)-**BIGI-3h** are shown in green and purple carbon atoms, respectively, important amino acid residues responsible for ligand anchoring in blue and catalytic triad in yellow. Distances are measured in angstroms (Å). 3D poses were generated using PyMOL viewer 2.4.1. Generally to 2D representation rendered in B and D - all the plausible interactions are dashed between appropriate amino acids and respective ligand parts. 2D diagrams were created with Discovery Studio Visualizer v. 20.1.0.19295 (BIOVIA, Dassault Systèmes, Release 2019, San Diego, USA).

On the contrary, (*S*)-**BIGI-3h** revealed slightly different orientation in *hAChE* active site (Figure 2 C, D). In similar fashion, Trp286 is implicated in π - π and cation- π interactions with *N*-benzyl moiety (4.3 Å) and nitrogen from piperidine (4.6 Å), respectively. Also methyl and ethyl-carboxylate appendages from ethyl 6-methyl-2-oxo-1,2,3,4-tetrahydropyrimidine-5-carboxylate displayed π -alkyl contacts to Tyr341, Tyr337, Trp86 and Phe338. 6,8-Dichloro-4*H*-chromen-4-one demonstrated only displaced π - π interaction with Trp86 (4.3 Å). His447 and Ser203 were found to exert van der Waals forces and Tyr124 formed hydrogen contact carbonyl from this fragment. The other prominent interactions regarding 6,8-dichloro-4*H*-chromen-4-one core observed in (*R*)-**BIGI-3h**-*hAChE* complex were omitted in (*S*)-**BIGI-3h**-*hAChE* complex.

In our opinion, all these observations slightly favour the accommodation of (*R*)-**BIGI-3h** enantiomer over (*S*)-**BIGI-3h**. The crucial element in this process seems to be the orientation of 6,8-dichloro-4*H*-

chromen-4-one moiety in the CAS of *hAChE*. These findings are also supported by the calculated energies used as scoring function where the binding affinities were estimated -13.4 kcal/mol and -12.3 kcal/mol for (*R*)-**BIGI-3h** and (*S*)-**BIGI-3h** enantiomers, respectively. Generally, weaker *hAChE* inhibition potency of (*R*)-**BIGI-3h** and (*S*)-**BIGI-3h** compared to donepezil might be attributed to inverted ligand anchoring in the gorge of the enzyme (Figure 3).

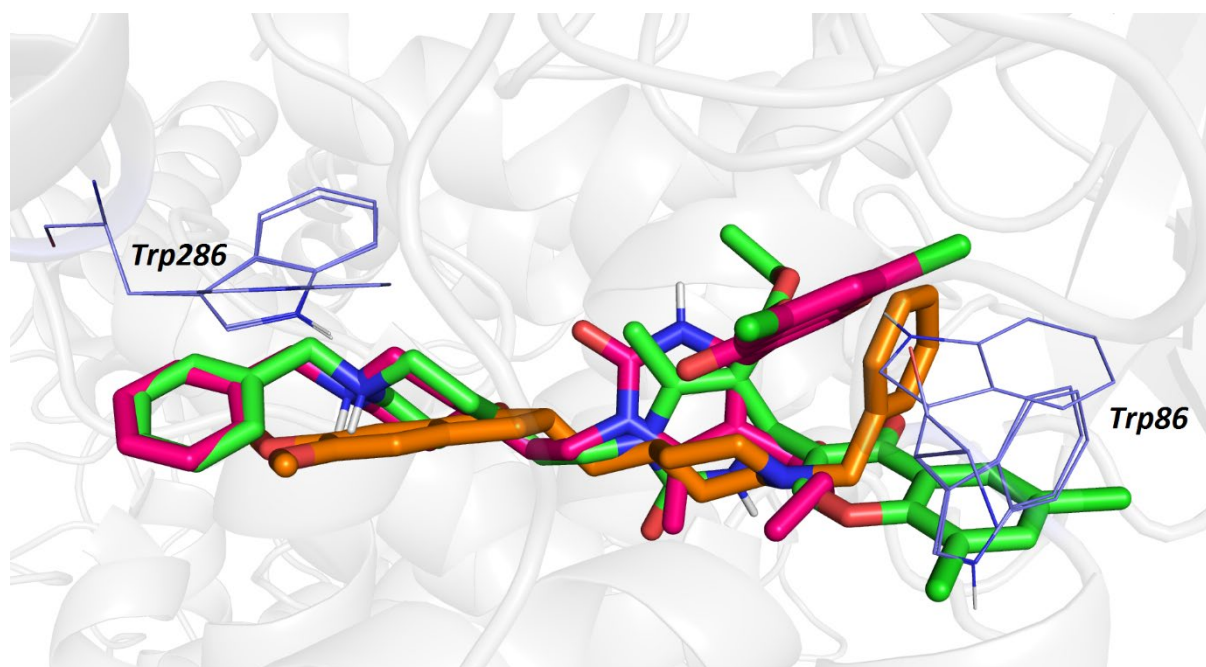


Figure 3. Spatial overlap between (*R*)-**BIGI-3h** (green), (*S*)-**BIGI-3h** (purple) and crystal structure of donepezil (orange) embedded within *hAChE* (PDB ID: 4EY7). For the sake of clarity, only Trp286 and Trp86 are displayed defining PAS and CAS regions of the enzyme, respectively.

MAO and GSK-3 β Inhibition Assays. MAO inhibitory activity was evaluated by the detection of the metabolites of a deamination of a MAO substrate by the MAO-A or B.⁵²The method used kynuramine as common substrate for both MAO A and B. The enzymes oxidize the substrate, which leading to 4-hydroxyquinoline (4-HQ) easily identified in the reaction medium by HPLC-MS (m/z 146 ion, $(M+H)^+$). Cloroglyline, an irreversible and selective MAOAI and Pargyline, an irreversible and selective MAOBI, were used as references. As shown in Table 3, although (+)-**BIGI-3h** and (-)-**BIGI-3h** showed weak MAO A inhibitory activity, both compounds could effectively inhibit MAO-B in the micromolar range, with IC_{50} of 11.2 and 12.34 μ M, respectively, compared with standard pargyline ($IC_{50} = 0.227 \mu$ M). GSK-3 β biochemical inhibition for (\pm)-**BIGI-3h**, (+)-**BIGI-3h**, and (-)-**BIGI-3h** was assessed using the Kinase-Glo luminescent assay, which quantifies the decrease in ATP levels following the kinase

reaction⁵³. SB-415286³⁴, a well-known GSK3 β inhibitor, was used as a positive control. As shown in Table 3, (\pm)-**BIGI-3h** and (-)-**BIGI-3h** showed similar IC₅₀ (29.1 and 24.3 μ M, respectively), whereas (+)-**BIGI-3h** was slightly more potent (IC₅₀ = 10.6 μ M). These activities within the micromolar range are in line with those of other multitarget-based GSK-3 β compounds³⁵.

Table 3. Efficacy of BIGI-3h and its enantiomers to inhibit hAChE, calcium channels, monoamine oxidase, and glycogen synthase kinase 3 β as well as A β ₁₋₄₂ and tau(306-336) aggregation, and the predicted BBB permeability of these compounds ^a							
Compounds	hAChE (IC ₅₀ μ M)	Calcium channel IC ₅₀ (μ M)	MAO A (IC ₅₀ μ M)	MAO-B (IC ₅₀ μ M)	A β ₁₋₄₂ aggregation (% inhibition) ^b	GSK-3 β (IC ₅₀ μ M)	τ (306-336) aggregation (% Inhibition) ^c
(\pm)- BIGI-3h	0.06 \pm 0.00	1.4 \pm 0.4	-	-	63.6 \pm 1.3	29.1 \pm 0.5	73.7 \pm 5.4
(+)- BIGI-3h [α_D] = 162° (c 0.14, MeOH)	0.09 \pm 0.00	5 \pm 2	75.6 \pm 35.7	11.2 \pm 1.09	66.5 \pm 0.9	10.6 \pm 1.5	78.3 \pm 3.0
(-)- BIGI-3h [α_D] = -178° (c 0.13, MeOH)	0.07 \pm 0.00	1.6 \pm 0.4	195 \pm 505	12.3 \pm 1.39	63.5 \pm 0.2	24.3 \pm 1.2	75.3 \pm 1.6
Clorgylin	-	-	0.045 \pm 0.003	-	-	-	-
Pargyline	-	-	-	0.227 \pm 0.029	-	-	-
SB-415286	-	-	-	-	-	0.055	-
Doxycycline	-	-	-	-	-	-	61.5 \pm 0.8

^aEach IC₅₀ and % values are the mean \pm standard error of mean of quadruplicate of at least three different experiments. ^b[A β] = [inhibitor] = 50 μ M; ^c [tau(306-336) peptide] = [inhibitor] = 50 μ M.

Tau Aggregation and Inhibition Study. As hyperphosphorylated tau aggregation seems to proceed in a manner similar to A β aggregation (conformational shift \rightarrow nucleation \rightarrow elongation), we evaluated the ability of (\pm)-**BIGI-3h** and its enantiomers to inhibit the aggregation of the tau(306-336) peptide comprising the R3 domain of tau protein, *in vitro*. The importance of the tau R3 domain in tau aggregation has been highlighted by a mutagenesis study⁵⁴. Furthermore, it has been recently shown that this fragment can induce the aggregation of tau microtubule-binding region in cells⁵⁵; thus, it represents a good *in vitro* model to monitor tau aggregation and screen for aggregation inhibitors.

Therefore, aggregation inhibition experiments were performed by incubating the tau(306-336) peptide in the absence or presence of the tested compounds at a concentration ratio of [inhib]/[tau] = 1/1 and equal to 50 μ M. Thioflavin T was used as a fluorescent dye to detect fibril formation. (\pm)-**BIGI-3h** showed an interesting inhibitory pattern: it delayed the lag phase ($t_{1/2}$ from 4.5 h to 6.3 h) (Figure 4) and inhibited tau(306-336) aggregation by 73.7%, while the anti-ChE drug tacrine did not significantly interfere with aggregation of the tau(306-336) peptide (Table 3). Doxycycline, which was used as

positive control, gave a percentage of inhibition of $61.5 \pm 0.8\%$, when assayed in the same experimental conditions (Table 3). A delay in the lag phase is an interesting feature for a potential inhibitor, as it implies potent inhibition in the early phase of tau aggregation and higher efficacy in preventing fibril formation. Pure enantiomers were tested under the same experimental conditions, but no significant difference in anti-tau aggregation activity was noted compared with that of the racemic mixture.

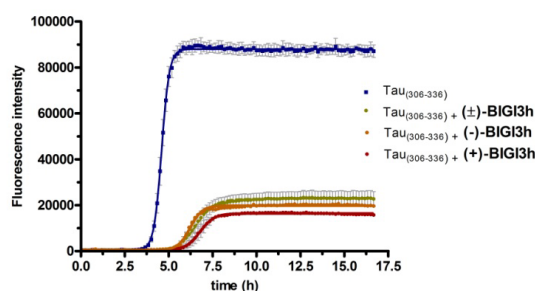


Figure 4. Inhibitory effects of compounds (\pm)-BIGI-3h, (+)-BIGI-3h, and (-)-BIGI-3h against the aggregation of tau(306-336) [tau(306-336) peptide] = [inhibitor] = 50 μ M. Aggregation is monitored by the increase in fluorescence emission in the presence of thioflavin T dye

In vivo study of BIGI-3h. (+)-BIGI-3h and (-)-BIGI-3h showed biological activity similar to that of the racemic mixture. Hence, an *in vivo* study was performed to obtain proof-of-concept regarding the brain activity of (\pm)-BIGI-3h, using the novel object recognition (NOR) test, a widely used test for cognition assessment⁵⁶. As expected, control mice (vehicle/DMSO group) spent more time exploring the novel object than the familiar one (RI=0,67, Figure 5). Compared with control treatment, scopolamine (1 mg/kg) treatment resulted in a decrease in the recognition index in mice, suggesting a working memory impairment. In fact, scopolamine produced a memory acquisition deficit, thus constituting an appropriate model to evaluate short-term memory. Importantly, mice treated with 10 mg/kg of (\pm)-BIGI-3h after scopolamine treatment showed significantly improved recognition index. These results showed that recognition memory deficits caused by scopolamine (1 mg/kg) injection are restored by 10 mg/kg of (\pm)-BIGI-3h (Figure 5). This activity can be likely mainly attributed to the anticholinesterase properties of this compound. It will nevertheless be interesting to identify the target engagement of (\pm)-BIGI-3h, through a comprehensive study on an appropriate animal model of Alzheimer's disease.

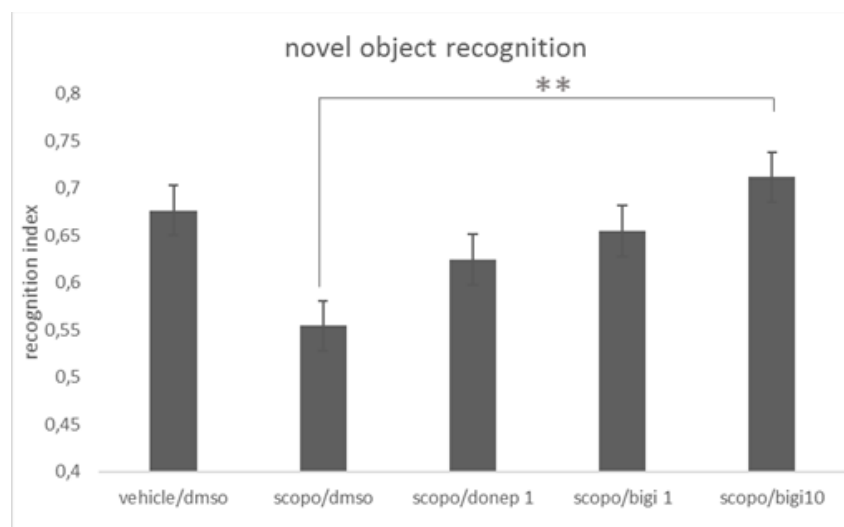


Figure 5. Effect of combined administration of scopolamine/dimethyl sulfoxide (scop/DMSO), donepezil, and (\pm)-**BIGI-3h** on recognition index. **BIGI 1**, 1 mg/kg; **BIGI 10**, 10 mg/kg. ** $p <$ corrected significance threshold.

CONCLUSION

Based on our confidence that MCRs represent a useful tool in medicinal chemistry and symbolize the most appropriate method for accessing to many different types of pharmacophores thus expressing particular relevance for the discovery of bioactive compounds, we have designed and synthesized *via* the Biginelli multicomponent reaction fourteen new compounds. From all the biological and physico-chemical results gathered in this study, we have identified (\pm) *ethyl 1-(2-(1-benzylpiperidin-4-yl)ethyl)-4-(6,8-dichloro-4-oxo-4H-chromen-3-yl)-6-methyl-2-oxo-1,2,3,4-tetrahydropyrimidine-5-carboxylate*. (\pm)-**BIGI-3h**, the first MTDL that simultaneously addressed several key targets involved in the AD pathological cascade.

This newly designed and well-balanced compound showed potent and well-balanced *in vitro* inhibitory activities against neurotransmitter-catabolizing enzymes (ChE and MAO) and GSK3 β kinase, along with VGCC blockade. (\pm)-**BIGI-3h** also showed potent inhibition of tau and A β aggregation, antioxidant activity, and good brain permeation. Moreover, BBB permeation was also confirmed by *in vivo* studies, which also showed that (\pm)-**BIGI-3h** (10 mg/kg) could significantly restore the cognitive deficit of scopolamine-treated mice in the NOR test. This beneficial activity can be likely mainly attributed to the anticholinesterase properties of this compound. Notwithstanding, specific AD murine models would be

required to further *in vivo* assess the multifunctional profile of (\pm) **BIGI-3h**, its unique pharmacological profile makes this compound eligible for further studies for a possible effective treatment of AD.

METHODS

Chemistry. *General Methods.* All the commercially available reagents and solvents were purchased from Sigma-Aldrich, VWR, and TCI. Reactions were followed by analytical thin layer chromatography (TLC) on precoated TLC plates (layer 0.20 mm silica gel 60 with a fluorescent indicator UV254). ^1H and ^{13}C NMR spectra were recorded on a Bruker spectrometer; operating at (^1H NMR at 400 MHz, ^{13}C NMR at 100 MHz), in solution in dimethylsulfoxide (DMSO- d_6) or Chloroform (CDCl_3) at 20°C; chemical shift values are given in δ (ppm) relatively to TMS as internal reference. Coupling constants are given in Hz. The following abbreviations were used: s = singlet, d = doublet, t = triplet, q = quartet, m = multiplet. High resolution mass spectra were obtained at Centre Commun de Spectrométrie de Masse, Lyon, France on a Bruker micrOTOF-Q II spectrometer (Bruker Daltonics) in positive ESI-TOF (electrospray ionization-time of flight). Elemental analyses were obtained by a Carlo Erba EA 1108 analyzer and the analytical results were within $\pm 0.2\%$ of the theoretical values for all compounds. The purity of the new compounds was checked by elemental analyses, conducted on a Carlo Erba EA 1108 apparatus, and confirmed to be $> 95\%$. The **BIGI** were found also to be $\geq 95\%$ pure by HPLC analysis using a Hitachi Lachrom Elite series instrument equipped with a L2400 Lachrom Elite DAD detector and a Uptisphere ODB column (4.6 mm x 100 mm, $\text{Ø} = 3\ \mu\text{m}$). Peaks were detected at 210 nm and the system was operated at 25°C with a flow rate of 2 mL/min. The mobile phase was an isocratic mixture of acetonitrile and water (1:1, v/v) containing 0.1% (w/v) of monopotassium phosphate.

Analyses by chiral SFC were run on Waters SFC/MS equipped with a UV_DAD (220 and 254 nm) detector and MS (APCI: +/- modes). Analyses were performed isocratic on a Chiralpak AS-H (4.6 x 100 mm, particle size 5 μm) with flow rate of 5 ml/min. Mobile phase was 0.2% Isopropylamine CO_2/EtOH (55:45). Separations by preparative chiral SFC were run on a Sepiatec Prep 100 SFC equipped with UV_DAD and a Chiralpak AS-H column (21 x 250 mm, particle size 5 μm). Peaks were detected at 220 and 254 nm and the system was operated at 40°C with a flow rate of 65 mL/min with the same mobile phase.

PAINS Analysis. The undetected Pan Assay INterference compounds (PAINS) with false-positive activities seriously compromise their outcomes in medicinal chemistry programs. Thus, although our designed and synthesized **BIGI**s are not known as classes of PAINS⁵⁷⁻⁶⁰, **BIGI-3h** was submitted to Free ADME-Tox filtering tool (FAFDrugs4) program (<http://fafdrugs4.mti.univ-paris-diderot.fr/>) and to the “False Positive Remover” software (<http://www.cbligand.org/PAINS/>). The results indicate that it is not classified as PAINS. **BIGI-3h** was not recognized also as PAINS according to swissadme.ch (see figure S27 in supporting Information). Finally, compound **BIGI-3h** showed 71% of similarity with a previously reported aggregator^{61,62} according to the software “Aggregator Advisor” (<http://advisor.bkslab.org/>). Then and since the aggregators are nonspecific inhibitors, **BIGI-3h** was evaluated against an unrelated enzyme (the Alkaline phosphatase, see Supporting information). The results indicated no inhibition, then proving that **BIGI-3h** is not an aggregator. In addition, the previously reported aggregator showed another chemical structure compared to our compounds, exhibiting a higher molecular weight equal to 840 g.mol⁻¹ and many conjugated double bonds (2 biphenyl groups with a total of five benzene rings in its structure)

Chemical Synthesis. General procedure for the synthesis of ureas 2a-c³⁷. To a solution of the corresponding 4-amino-benzylpiperidine (1 g) in dichloromethane (10 mL) at 0°C was added a 20 mL solution of benzoyl isocyanate (1.2 eq.) in dichloromethane. The reaction was stirred for 1 hour at room temperature. The solvent was evaporated and the crude oil was recrystallized in diethyl ether to give a white solid. Yield: 72%. The product was reacted without further purification.

The corresponding benzoyl compound was hydrolyzed 48 hours at room temperature in a 1:1 solution of methanol in 1 M aqueous NaOH (30 mL). The solvents were concentrated under vacuum and extracted 3 times with ethyl acetate. The combined organic layers were washed with brine, dried over Na₂SO₄ and evaporated. The obtained solid was washed with diethyl ether to give a white solid. Yields: 41 to 55%.

1-((1-benzylpiperidin-4-yl)methyl)urea (**2a**)

Yield: 41 % ¹H NMR (400 MHz, CDCl₃) δ 7.36 – 7.30 (m, 4H), 7.28 – 7.23 (m, 1H), 5.03 (bs, 1H), 4.60 (s, 2H), 3.50 (s, 2H), 3.10 – 3.00 (m, 2H), 2.95 – 2.85 (m, 2H), 2.02 – 1.89 (m, 2H), 1.74 – 1.62 (m, 2H), 1.57 – 1.41 (m, 1H), 1.37 – 1.21 (m, 2H).

1-(2-(1-benzylpiperidin-4-yl)ethyl)urea (**2b**)

Yield: 43 %. ¹H NMR (400 MHz, CDCl₃) δ 7.36 – 7.30 (m, 4H), 7.28 – 7.23 (m, 1H), 4.67 (bs, 1H), 4.46 (bs, 2H), 3.50 (s, 2H), 3.25 – 3.13 (m, 2H), 2.94 – 2.82 (m, 2H), 2.03 – 1.87 (m, 2H), 1.73 – 1.59 (m, 2H), 1.50 – 1.40 (m, 2H), 1.37 – 1.22 (m, 3H).

1-(3-(1-benzylpiperidin-4-yl)propyl)urea (**2c**)

Yield: 35 %. ¹H NMR (400 MHz, CDCl₃) δ 7.29 – 7.26 (m, 5H), 4.45 (bs, 1H), 4.35 (bs, 2H), 3.47 (s, 2H), 3.16 – 3.10 (m, 2H), 2.88 – 2.84 (m, 2H), 1.95 – 1.87 (m, 2H), 1.65 – 1.53 (m, 2H), 1.48 – 1.46 (m, 2H). 1.27 – 1.19 (m, 5H).

General procedure for the synthesis of Biginelli compounds BIGI-3a-n. To a solution of 150 mg of the corresponding commercially chromones in 10 mL of acetic acid was added 1.2 equivalent of the corresponding urea 2a-c. The reaction was stirred for 2h. 1.25 equivalent of ethyl acetoacetate and 1 equivalent of sodium bisulfate were added. The reaction was stirred for 60 hours at room temperature and then refluxed 4h. The catalyst was filtered off and the solvent was evaporated under vacuum. The crude oil was purified by flash chromatography eluted with dichloromethane/MeOH/NH₃(aq) 96:4:0.4 to give the pure product. Yield 45-78%.

(±) *Ethyl 1-((1-benzylpiperidin-4-yl)methyl)-6-methyl-2-oxo-4-(4-oxo-4H-chromen-3-yl)-1,2,3,4-tetrahydro pyrimidine-5-carboxylate* **BIGI-3a**. Following the general procedure compound **BIGI-3a** was obtained as a brown powder with a yield of 52%. ¹H NMR (400 MHz, CDCl₃) δ 8.24-8.21 (dd, 1H), 7.65-7.72 (m, 1H), 7.63 (s, 1H), 7.45-7.42 (m, 2H), 7.29-7.26 (m, 5H), 6.02-6.01 (dd, 1H), 5.61-5.60 (dd, 1H), 4.18-4.08 (m, 2H), 4.07-3.99 (m, 1H), 3.47 (s, 2H), 3.36-3.31 (dd, 1H), 2.88-2.77 (dd, 2H), 2.59 (s, 3H), 1.95-1.86 (m, 3H), 1.61-1.47 (m, 2H), 1.33-1.26 (m, 2H), 1.19-1.16 (t, 3H). ¹³C NMR (101 MHz, CDCl₃) δ 176.55, 164.65, 162.42, 155.45, 152.67, 151.65, 150.90, 133.01, 128.28, 127.27, 124.83, 124.44, 122.90, 122.27, 117.15, 98.88, 59.44, 51.88, 45.81, 28.67, 15.54, 13.24. Anal. Calcd. for C₃₀H₃₃N₃O₅: C, 69.88; H, 6.45; N, 8.15; found: C, 70.05; H, 6.51; N, 7.99.

(±) Ethyl 1-((1-benzylpiperidin-4-yl)methyl)-4-(6-bromo-4-oxo-4H-chromen-3-yl)-6-methyl-2-oxo-1,2,3,4-tetrahydropyrimidine-5-carboxylate **BIGI-3b**. Following the general procedure compound **BIGI-3b** was obtained as a brown yellow powder with a yield of 63%. ¹H NMR (400 MHz, CDCl₃) δ 8.27-8.26 (d, 1H), 7.69-7.66 (dd, 1H), 7.55 (s, 1H), 7.26-7.16 (m, 6H), 5.97-5.96 (d, 1H), 5.48-5.47 (d, 1H), 4.10-3.99 (m, 2H), 3.52-3.89 (m, 1H), 3.49-3.37 (m, 3H), 2.79-2.75 (m, 2H), 2.51 (s, 3H), 1.79-1.75 (m, 2H), 1.59-1.51 (m, 3H), 1.22-1.15 (m, 2H), 1.19-1.15 (m, 3H). ¹³C NMR (101 MHz, CDCl₃) δ 176.17, 165.57, 155.21, 153.48, 153.03, 151.85, 137.83, 136.97, 129.31, 128.47, 128.18, 127.08, 125.25, 123.67, 120.15, 118.88, 99.53, 63.15, 60.43, 53.47, 46.60, 40.58, 36.52, 33.64, 32.07, 31.73, 16.11, 14.30. Anal. Calcd. for C₃₀H₃₂BrN₃O₅: C, 60.61; H, 5.43; N, 7.07; Br, 13.44; found: C, 60.52; H, 5.48; N, 7.12; Br, 13.37.

(±) Ethyl 1-((1-benzylpiperidin-4-yl)methyl)-4-(7-ethyl-4-oxo-4H-chromen-3-yl)-6-methyl-2-oxo-1,2,3,4-tetrahydropyrimidine-5-carboxylate **BIGI-3c**. Following the general procedure compound **BIGI-3c** was obtained as a purple powder with a yield of 78%. ¹H NMR (400 MHz, CDCl₃) δ 7.96-7.95 (d, 1H), 7.53 (s, 1H), 7.45-7.43 (dd, 1H), 7.29-7.27 (m, 1H), 7.21-7.15 (m, 5H), 5.97-5.95 (d, 1H), 5.54-5.53 (d, 1H), 4.10-3.92 (m, 3H), 3.37 (s, 2H), 3.28-3.23 (dd, 1H), 2.78-2.66 (m, 4H), 2.51 (s, 3H), 1.84-1.75 (m, 2H), 1.48-1.37 (m, 3H), 1.27-1.17 (m, 5H), 1.11-1.08 (t, 3H). ¹³C NMR (101 MHz, CDCl₃) δ 177.64, 165.73, 154.94, 153.78, 152.55, 151.95, 141.83, 134.30, 129.19, 128.20, 127.11, 123.91, 123.69, 123.06, 118.02, 100.04, 62.91, 60.43, 52.85, 47.08, 46.77, 36.71, 29.72, 28.39, 16.51, 15.54, 14.28. Anal. Calcd. for C₃₂H₃₇N₃O₅: C, 70.70; H, 6.86; N, 7.73; found: C, 70.85; H, 6.81; N, 7.69.

(±) Ethyl 1-(2-(1-benzylpiperidin-4-yl)ethyl)-6-methyl-2-oxo-4-(4-oxo-4H-chromen-3-yl)-1,2,3,4-tetrahydro pyrimidine-5-carboxylate **BIGI-3d**. Following the general procedure compound **BIGI-3d** was obtained as a red powder with a yield of 45%. ¹H NMR (400 MHz, CDCl₃) δ 8.25-8.22 (d, 1H), 7.72-7.67 (t, 1H), 7.61 (s, 1H), 7.46-7.43 (m, 2H), 7.28-7.26 (m, 5H), 5.97-5.96 (d, 1H), 5.59-5.58 (d, 1H), 4.19-4.06 (m, 2H), 3.98-3.92 (m, 1H), 3.60-3.5 (m, 1H), 3.42 (s, 2H), 2.85-2.81 (d, 2H), 2.6 (s, 3H), 1.85-1.75 (m, 2H), 1.70-1.67 (m, 1H), 1.62-1.53 (m, 2H), 1.42-1.33 (m, 1H), 1.29-1.27 (m, 3H), 1.25-1.15 (m, 3H). ¹³C NMR (101 MHz, CDCl₃) δ 177.52, 165.64, 156.48, 153.58, 152.75, 151.80, 134.00, 129.27, 128.17, 127.06, 125.85, 125.43, 123.95, 123.31, 118.20, 99.70, 63.23, 60.38, 53.56,

53.52, 46.56, 40.46, 36.51, 33.59, 32.11, 31.72, 31.64, 29.70, 16.07, 14.27. Anal. Calcd. for C₃₁H₃₅N₃O₅: C, 70.30; H, 6.66; N, 7.93; found: C, 70.11; H, 6.72; N, 7.99.

(±) *Ethyl 1-(2-(1-benzylpiperidin-4-yl)ethyl)-4-(6-bromo-4-oxo-4H-chromen-3-yl)-6-methyl-2-oxo-1,2,3,4-tetrahydropyrimidine-5-carboxylate* **BIGI-3e**. Following the general procedure compound **BIGI-3e** was obtained as a brown powder with a yield of 68%. ¹H NMR (400 MHz, CDCl₃) δ 8.33 (s, 1H), 7.75-7.73 (d, 1H), 7.61 (s, 1H), 7.33-7.26 (m, 6H), 6.03-6.02 (d, 1H), 5.54-5.53 (d, 1H), 4.14-4.06 (m, 2H), 3.94-3.91 (m, 1H), 3.59-3.50 (m, 1H), 3.42 (s, 2H), 2.84-2.80 (d, 2H), 2.58 (s, 3H), 1.83-1.80 (m, 2H), 1.68-1.57 (m, 3H), 1.24-1.18 (m, 4H), 1.16-1.14 (m, 3H). ¹³C NMR (101 MHz, CDCl₃) δ 176.17, 165.55, 155.19, 153.46, 153.02, 151.80, 137.40, 136.97, 129.39, 128.44, 128.20, 127.18, 125.22, 123.62, 120.14, 118.88, 99.51, 63.04, 60.43, 53.38, 53.34, 46.58, 40.55, 36.45, 33.55, 31.90, 31.56, 16.11, 14.27. Anal. Calcd. for C₃₁H₃₄BrN₃O₅: C, 61.19; H, 5.63; N, 6.91; Br, 13.13; found: C, 61.42; H, 5.49; N, 6.84; Br, 13.05.

(±) *Ethyl 1-(2-(1-benzylpiperidin-4-yl)ethyl)-4-(7-ethyl-4-oxo-4H-chromen-3-yl)-6-methyl-2-oxo-1,2,3,4-tetrahydropyrimidine-5-carboxylate* **BIGI-3f**. Following the general procedure compound **BIGI-3f** was obtained as a brown powder with a yield of 57%. ¹H NMR (400 MHz, CDCl₃) δ 7.96-7.95 (d, 1H), 7.53 (s, 1H), 7.46-7.43 (dd, 1H), 7.29-7.15 (m, 6H), 5.96-5.95 (d, 1H), 5.51-5.50 (d, 1H), 4.10-3.99 (m, 2H), 3.85-3.95 (m, 1H), 3.50-3.45 (m, 1H), 3.34 (s, 2H), 2.77-2.66 (m, 4H), 2.52 (s, 3H), 1.77-1.74 (m, 2H), 1.62-1.59 (m, 1H), 1.54-1.51 (m, 2H), 1.30-1.35 (m, 2H), 1.17-1.23 (m, 5H), 1.11-1.08 (t, 3H). ¹³C NMR (101 MHz, CDCl₃) δ 177.64, 165.68, 154.93, 153.64, 152.66, 151.76, 141.79, 138.00, 134.26, 129.27, 128.17, 127.04, 123.91, 123.74, 123.11, 118.05, 99.83, 63.24, 60.35, 53.57, 53.53, 46.62, 40.45, 36.53, 33.60, 32.15, 31.74, 28.39, 16.07, 15.57, 14.28. Anal. Calcd. for C₃₃H₃₉N₃O₅: C, 71.07; H, 7.05; N, 7.53; found: C, 70.95; H, 7.11; N, 7.62.

(±) *Ethyl 1-(2-(1-benzylpiperidin-4-yl)ethyl)-4-(6-chloro-7-methyl-4-oxo-4H-chromen-3-yl)-6-methyl-2-oxo-1,2,3,4-tetrahydropyrimidine-5-carboxylate* **BIGI-3g**. Following the general procedure compound **BIGI-3g** was obtained as a purple powder with a yield of 66%. ¹H NMR (400 MHz, CDCl₃) δ 8.15 (s, 1H), 7.5 (s, 1H), 7.31-7.27 (m, 6H), 6.03-6.02 (d, 1H), 5.54-5.53 (d, 1H), 4.16-4.08 (m, 2H), 3.9 (m, 1H), 3.58-3.48 (m, 3H), 2.90-2.87 (d, 2H), 2.57 (s, 3H), 2.48 (s, 3H), 2.01 (s, 1H), 1.90-1.86 (d,

2H), 1.67-1.58 (m, 3H), 1.27-1.24 (m, 3H), 1.18-1.13 (m, 3H). ¹³C NMR (101 MHz, CDCl₃) δ 176.28, 165.58, 154.71, 153.53, 152.78, 151.70, 143.38, 137.04, 132.17, 129.49, 128.22, 127.26, 125.43, 123.29, 122.98, 119.93, 99.64, 62.82, 60.39, 53.20, 53.15, 46.57, 40.49, 36.42, 33.47, 31.74, 31.38, 20.87, 16.09, 14.26. Anal. Calcd. for C₃₂H₃₆ClN₃O₅: C, 66.48; H, 6.28; N, 7.27; Cl, 6.13; found: C, 66.34; H, 6.35; N, 7.18; Cl, 6.24.

(±) *Ethyl 1-(2-(1-benzylpiperidin-4-yl)ethyl)-4-(6,8-dichloro-4-oxo-4H-chromen-3-yl)-6-methyl-2-oxo-1,2,3,4-tetrahydropyrimidine-5-carboxylate* **BIGI-3h**. Following the general procedure compound **BIGI-3h** was obtained as a brown yellow powder with a yield of 75%. ¹H NMR (400 MHz, CDCl₃) δ 8.10-8.09 (d, J = 4.0 Hz, 1H), 7.75-7.74 (d, 2H), 7.37-7.34 (m, 5H), 6.16-6.15 (d, 1H), 5.54-5.53 (d, 1H) 4.20 – 4.10 (m, 2H), 3.88 – 3.86 (m, 1H), 3.76 (s, 2H), 3.66 – 3.57 (m, 1H), 3.19 – 3.16 (m, 2H), 2.59 (s, 3H), 2.23-2.18 (m, 2H), 1.79 – 1.72 (m, 2H), 1.62 – 1.59 (m, 3H), 1.57-1.55 (m, 1H), 1.20 (m, 1H), 1.18 (t, J = 8.0 Hz, 3H). ¹³C NMR (101 MHz, CDCl₃) δ 176.00, 175.75, 165.49, 153.70, 153.20, 151.69, 150.88, 134.24, 131.29, 130.58, 128.77, 125.82, 124.58, 124.10, 123.90, 99.51, 61.56, 60.67, 52.32, 46.85, 40.53, 36.04, 32.81, 30.28, 29.95, 22.12, 16.26, 14.38. HRMS ESI-TOF [M+H]⁺ m/z meas. for C₃₁H₃₄Cl₂N₃O₅ : 598.1862, found: 598.1870. Anal. Calcd. for C₃₁H₃₃Cl₂N₃O₅: C, 62.21; H, 5.56; N, 7.02; Cl, 11.85; found: C, 62.38; H, 5.47; N, 7.13; Cl, 11.74.

(+) *Ethyl 1-(2-(1-benzylpiperidin-4-yl)ethyl)-4-(6,8-dichloro-4-oxo-4H-chromen-3-yl)-6-methyl-2-oxo-1,2,3,4-tetrahydropyrimidine-5-carboxylate* (+) **BIGI-3h**. Retention time on analytical chiral HPLC: 0.48 min. [α]_D = + 162° (c 0.14, MeOH), HRMS ESI-TOF [M+H]⁺ m/z meas. for C₃₁H₃₄Cl₂N₃O₅ : 598.1872, found: 598.1870.

(-) *Ethyl 1-(2-(1-benzylpiperidin-4-yl)ethyl)-4-(6,8-dichloro-4-oxo-4H-chromen-3-yl)-6-methyl-2-oxo-1,2,3,4-tetrahydropyrimidine-5-carboxylate* (-) **BIGI-3h**. Retention time on analytical chiral HPLC: 0.72 min [α]_D = - 178° (c 0.13, MeOH), HRMS ESI-TOF [M+H]⁺ m/z meas. for C₃₁H₃₄Cl₂N₃O₅ : 598.1874, found: 598.1870.

(±) *Ethyl 1-(3-(1-benzylpiperidin-4-yl)propyl)-6-methyl-2-oxo-4-(4-oxo-4H-chromen-3-yl)-1,2,3,4-tetrahydropyrimidine-5-carboxylate* **BIGI-3i**. Following the general procedure compound **BIGI-3i** was obtained as a brown powder with a yield of 55%. ¹H NMR (400 MHz, CDCl₃) δ 8.16-8.14 (dd, 1H), 7.62-7.55 (m, 2H), 7.37-7.33 (m, 2H), 7.24-7.16 (m, 5H), 5.93-5.92 (dd, 1H), 5.52-5.51 (dd, 1H), 4.11-

3.99 (m, 2H), 3.75-3.80 (m, 1H), 3.47-3.43 (m, 3H), 2.81-2.78 (m, 2H), 2.53 (s, 3H), 1.89-1.83 (t, 2H), 1.53-1.49 (m, 3H), 1.35-1.45 (m, 1H), 1.18-1.08 (m, 8H). ¹³C NMR (101 MHz, CDCl₃) δ 177.54, 165.69, 156.48, 153.62, 152.75, 151.87, 134.01, 129.39, 127.11, 125.85, 125.43, 123.95, 123.33, 118.18, 99.55, 63.17, 60.39, 53.62, 53.57, 46.59, 42.75, 35.28, 33.42, 31.99, 37.29, 16.17, 14.28. Anal. Calcd. for C₃₂H₃₇N₃O₅: C, 70.70; H, 6.86; N, 7.73; found: C, 70.58; H, 6.92; N, 7.70.

(±) *Ethyl 1-(3-(1-benzylpiperidin-4-yl)propyl)-4-(6-bromo-4-oxo-4H-chromen-3-yl)-6-methyl-2-oxo-1,2,3,4-tetrahydropyrimidine-5-carboxylate* **BIGI-3j**. Following the general procedure compound **BIGI-3j** was obtained as a brown powder with a yield of 49%. ¹H NMR (400 MHz, CDCl₃) δ 8.28-8.27 (d, 1H), 7.68-7.66 (dd, 1H), 7.55 (s, 1H), 7.27-7.18 (m, 6H), 5.86-5.85 (d, 1H), 5.50-5.49 (d, 1H), 4.11-3.99 (m, 2H), 3.78 (m, 1H), 3.45-3.41 (m, 2H), 3.48 (s, 1H), 2.81-2.76 (m, 2H), 2.53 (s, 3H), 1.87-1.81 (t, 2H), 1.53-1.49 (m, 3H), 1.35-1.40 (m, 1H), 1.12-1.09 (m, 8H). ¹³C NMR (101 MHz, CDCl₃) δ 176.25, 165.60, 155.23, 153.46, 152.96, 151.98, 137.01, 129.29, 128.47, 128.16, 127.01, 125.23, 123.62, 120.14, 118.91, 99.32, 63.35, 60.44, 53.76, 46.57, 42.83, 35.46, 33.49, 32.18, 27.28, 16.20, 14.28. Anal. Calcd. for C₃₂H₃₆BrN₃O₅: C, 61.74; H, 5.83; N, 6.75; Br, 12.83; found: C, 61.82; H, 5.77; N, 6.81; Br, 12.74.

(±) *Ethyl 1-(3-(1-benzylpiperidin-4-yl)propyl)-4-(7-ethyl-4-oxo-4H-chromen-3-yl)-6-methyl-2-oxo-1,2,3,4-tetrahydropyrimidine-5-carboxylate* **BIGI-3k**. Following the general procedure compound **BIGI-3k** was obtained as a brown powder with a yield of 63%. ¹H NMR (400 MHz, CDCl₃) δ 7.96-7.95 (d, 1H), 7.53 (s, 1H), 7.45-7.42 (dd, 1H), 7.29-7.19 (m, 6H), 5.91-5.90 (d, 1H), 5.52-5.51 (d, 1H), 4.10-3.99 (m, 2H), 3.77-3.81 (m, 1H), 3.45-3.50 (m, 3H), 2.88-2.81 (d, 2H), 2.72-2.66 (dd, 2H), 2.53 (s, 3H), 1.82-1.90 (m, 1H), 1.52-1.50 (m, 3H), 1.42-1.45 (m, 1H), 1.23-1.08 (m, 12H). ¹³C NMR (101 MHz, CDCl₃) δ 177.68, 165.71, 154.93, 153.65, 152.62, 151.82, 141.79, 134.28, 129.43, 129.37, 128.23, 127.20, 127.19, 123.89, 123.72, 123.09, 118.03, 99.64, 63.17, 63.15, 60.36, 53.63, 53.59, 46.62, 42.71, 35.31, 33.36, 31.94, 31.93, 31.91, 31.88, 29.72, 28.39, 27.28, 16.16, 15.54, 14.28. Anal. Calcd. for C₃₄H₄₁N₃O₅: C, 71.43; H, 7.23; N, 7.35; found: C, 71.35; H, 7.28; N, 7.44.

(±) *Ethyl 1-(3-(1-benzylpiperidin-4-yl)propyl)-4-(6-chloro-7-methyl-4-oxo-4H-chromen-3-yl)-6-methyl-2-oxo-1,2,3,4-tetrahydropyrimidine-5-carboxylate* **BIGI-3l**. Following the general procedure

compound **BIGI-3l** was obtained as a brown yellow powder with a yield of 62%. ¹H NMR (400 MHz, CDCl₃) δ 8.33 (s, 1H), 7.75 (s, 1H), 7.24-7.16 (m, 6H), 5.88-5.87 (d, 1H), 5.50-5.49 (d, 1H), 4.10-3.99 (m, 2H), 3.78-3.58 (m, 1H), 3.47-3.42 (m, 3H), 2.79-2.77 (d, 2H), 2.52 (s, 3H), 2.41 (s, 3H), 1.87-1.82 (t, 2H), 1.54-1.49 (m, 3H), 1.35-1.45 (m, 1H), 1.18-1.08 (m, 8H). ¹³C NMR (101 MHz, CDCl₃) δ 176.36, 165.64, 154.75, 153.52, 152.76, 151.89, 143.41, 132.20, 129.29, 128.17, 127.02, 125.45, 123.31, 122.99, 119.93, 99.44, 63.33, 60.40, 53.71, 46.54, 42.80, 35.46, 33.46, 32.15, 27.28, 20.87, 16.18, 14.28. Anal. Calcd. for C₃₃H₃₈ClN₃O₅: C, 66.94; H, 6.47; N, 7.10; Cl, 5.99; found: C, 67.90; H, 6.43; N, 7.19; Cl, 5.98.

(±) *Ethyl 1-(3-(1-benzylpiperidin-4-yl)propyl)-4-(6,8-dichloro-4-oxo-4H-chromen-3-yl)-6-methyl-2-oxo-1,2,3,4-tetrahydropyrimidine-5-carboxylate* **BIGI-3m**. Following the general procedure compound **BIGI-3m** was obtained as a brown powder with a yield of 49%. ¹H NMR (101 MHz, CDCl₃) δ 8.03-8.02 (d, 1H), 7.66-7.64 (dd, 2H), 7.25-7.18 (m, 5H), 5.83-5.82 (d, 1H), 5.49-5.48 (d, 1H), 4.12-4.00 (m, 2H), 3.70-3.80 (m, 1H), 3.47-3.45 (m, 3H), 2.87-2.81 (m, 2H), 2.53 (s, 3H), 1.80-1.95 (m, 2H), 1.50-1.65 (m, 3H), 1.45-1.48 (m, 1H), 1.18-1.35 (m, 8H). ¹³C NMR (101 MHz, CDCl₃) δ 175.82, 165.46, 153.37, 152.99, 152.12, 150.80, 134.17, 131.21, 129.43, 128.24, 127.19, 125.69, 124.48, 124.00, 123.81, 99.05, 63.20, 60.52, 53.59, 46.56, 42.94, 35.35, 33.42, 31.94, 29.71, 27.28, 16.22, 14.30. Anal. Calcd. for C₃₂H₃₅Cl₂N₃O₅: C, 62.75; H, 5.76; N, 6.86; Cl, 11.58; found: C, 62.98; H, 5.72; N, 6.74; Cl, 11.41.

(±) *Ethyl 1-(3-(1-benzylpiperidin-4-yl)propyl)-4-(6-isopropyl-4-oxo-4H-chromen-3-yl)-6-methyl-2-oxo-1,2,3,4-tetrahydropyrimidine-5-carboxylate* **BIGI-3n**. Following the general procedure compound **BIGI-3n** was obtained as a brown powder with a yield of 45%. ¹H NMR (400 MHz, CDCl₃) δ 7.98-7.97 (d, 1H), 7.54 (d, 2H), 4.46-7.50 (dd, 1H), 7.32-7.20 (m, 5H), 6.18-6.17 (d, 1H), 5.49-5.48 (d, 1H), 4.10-3.99 (m, 2H), 3.9 (s, 2H), 3.70-3.80 (m, 1H), 3.45-3.50 (m, 1H), 3.23-3.20 (m, 2H), 2.98-2.94 (m, 1H), 2.5 (s, 3H), 1.60-1.65 (m, 2H), 1.48-1.08 (m, 18H). ¹³C NMR (101 MHz, CDCl₃) δ 177.63, 165.65, 154.93, 153.87, 152.73, 151.41, 146.44, 133.04, 131.10, 130.91, 129.03, 129.82, 123.70, 123.05, 122.46, 118.06, 99.72, 80.62, 80.40, 51.80, 46.82, 42.58, 33.86, 32.47, 30.32, 29.70, 29.51, 29.40, 26.93,

23.94, 23.91, 16.16, 14.26. Anal. Calcd. for C₃₅H₄₃N₃O₅: C, 71.77; H, 7.40; N, 7.17; found: C, 72.03; H, 7.39; N, 7.09.

Biology. Measurement of cytosolic Ca²⁺ in SH-SY5Y cells. SH-SY5Y cells were maintained similarly to what was previously described⁶³. Free cytosolic Ca²⁺ was measured using the fluorescent Ca²⁺ indicator Fluo-4/AM (Fluo-4 acetoxymethyl ester). SH-SY5Y cells were seeded onto 96-well black plates at a density of 10⁵ cells per well, achieving confluence after 48 h. Cells were washed with Krebs-HEPES (KH) solution (KH, in mM: 144 NaCl, 5.9 KCl, 1.2 MgCl₂, 2 CaCl₂, 11 d-glucose, 10 HEPES, pH 7.4). Cells were loaded with 10 mM Fluo-4/AM and 0.2% pluronic acid in KH and incubated for 45 min at 37 °C in the dark. Then, cells were washed twice with KH to remove the excess of probe. Tested compounds were incubated 10 min before K⁺ 70 mM was applied to evoke the increment of cytosolic Ca²⁺. To normalize Fluo-4 signals, Triton X-100 (5%) and 1 M MnCl₂ were applied to register both maximal and minimal fluorescence, respectively. The experiments were analyzed at excitation and emission wavelengths of 485 and 520 nm, respectively, and fluorescence was measured in a fluorescence microplate reader (FLUOstar Optima, BMG, Germany). Data were calculated as a percentage of $F_{\max} - F_{\min}$.

In vitro anti-cholinesterase assay. The AChE and BuChE inhibitory activity of the tested compounds was determined using a modified Ellman's method³⁸ Human erythrocytes acetylcholinesterase (*hAChE*; EC 3.1.1.7), and human recombinant butyrylcholinesterase (*hBuChE*; EC 3.1.1.8), 5,5'-dithiobis(2-nitrobenzoic acid) (Ellman's reagent, DTNB), phosphate buffer (PB, pH 7.4), acetylthiocholine (ATC), and butyrylthiocholine (BTC), were purchased from Sigma-Aldrich (Prague, Czech Republic). Nunc polystyrene 96-well microplates with flat-bottom shape (ThermoFisher Scientific, USA) were used for the measurement and all the assay were carried out in 0.1 M KH₂PO₄/K₂HPO₄ buffer, pH 7.4. Enzyme solution was prepared at activity 2.0 units/mL in 2 mL aliquots. The assay mixture (100 μL) consisted of 40 μL of 0.1 M phosphate buffer (pH 7.4), 20 μL of 0.01 M DTNB, 10 μL of enzyme, and 20 μL of 0.01 M substrate (ATC iodide solution). Tested compounds were dissolved first in methanol or in DMSO and then further diluted by assay buffer to the final concentration. The highest concentration

tested was 31.6 μM , which contained 0.5% of co-solvent (methanol or DMSO) in the assay mixture. Such level of co-solvents was proved to have no effect on the activity of the enzyme. Enzyme with the inhibitor was preincubated for 5 min in the assay mixture and then the reaction was started by addition of 20 μL of substrate (ATC for AChE, BTC for BChE). The enzyme activity was determined by measuring the increase in absorbance at 412 nm at 37 °C in 2 min intervals using a Multi-mode microplate reader Synergy 2 (Vermont, USA). Each concentration was assayed in triplicate. The obtained data were used to compute the percentage inhibition (I ; Equation 1):

$$I = 1 - \frac{\Delta A_i}{\Delta A_0} \quad [\%] \quad (\text{Eq. 1})$$

ΔA_i indicates the absorbance change provided by cholinesterase exposed to AChE inhibitors and ΔA_0 indicates absorbance change caused by intact cholinesterase (phosphate buffer was used instead of AChE inhibitor solution). The inhibition potency of the tested compounds was expressed as IC_{50} value (the concentration of inhibitor which causes 50% cholinesterase inhibition). Calculations were performed using software Microsoft Excel (Redmont, WA, USA) and GraphPad Prism version 5.02 for Windows, GraphPad Software, San Diego, CA, USA.

Oxygen Radical Absorbance Capacity Assay (ORAC). The radical scavenging capacity of the TFAHs was determined by the ORAC-FL method using fluorescein as a fluorescent probe.^{41,42} A Varioskan Flash plate reader with built-in injectors (Thermo Scientific) was used. The reaction was carried out at 37 °C in 75 mM phosphate buffer (pH= 7.4) and the final volume reaction mixture was 200 μL . In a black 96-well microplate (Nunc), antioxidant (20 μL) and fluorescein (FL, 120 μL , final concentration of 70 nM) were incubated for 15 min at 37 °C. Then, 2,2'-azobis(amidinopropane) dihydrochloride (AAPH, 60 μL , final concentration of 40 mM) solution was added rapidly using the built-in injector. The fluorescence was measured every minute for 60 min at 485 nm (excitation wavelength) and 535 nm (emission wavelength). All the reactions were made in triplicate and at least three different assays were performed for each sample. Antioxidant curves (fluorescence versus time) were first normalized to the curve of the blank (without antioxidant) and then, the area under the

fluorescence decay curve (AUC) was calculated as: $AUC = 1 + \sum (f_i/f_0)$, Where f_0 is the initial fluorescence reading at 0 min and f_i is the fluorescence value at time i .

The net AUC corresponding to a sample was calculated as follows:

$$\text{Net AUC} = \text{AUC}_{\text{antioxidant}} - \text{AUC}_{\text{blank}}$$

Regression equations were calculated by plotting the net AUC against the antioxidant concentration. The ORAC value was obtained by dividing the slope of the latter curve between the slope of the Trolox curve obtained in the same assay. Final ORAC values were expressed as μmol of Trolox equivalent/ μmol .

Inhibition of $A\beta_{1-42}$ self-aggregation. 1,1,1,3,3,3-Hexafluoro-2-propanol (HFIP) pre-treated $A\beta_{1-42}$ samples (Bachem AG, Switzerland) were resolubilized with a MeCN/0.3 mM Na_2CO_3 /250 mM NaOH (48.4/48.4/3.2) mixture to have a stable stock solution ($[A\beta_{1-42}] = 500 \mu\text{M}$).⁴³ Experiments were performed by incubating the peptide in 10 mM phosphate buffer (pH 8.0) containing 10 mM NaCl, at 30 °C for 24 h (final $A\beta$ concentration = 50 μM with and without inhibitor (50 μM). The inhibitor was dissolved in methanol and diluted in the assay buffer. Blanks containing inhibitor and ThT were also prepared and evaluated to account for quenching and fluorescence properties. To quantify amyloid fibril formation, the ThT fluorescence method was used.^{64,65} After incubation, samples were diluted to a final volume of 2.0 mL with 50 μM glycine-NaOH buffer (pH 8.5) containing 1.5 μM ThT. A 300-s scan of fluorescence intensity was carried out ($\lambda_{\text{exc}} = 446 \text{ nm}$; $\lambda_{\text{em}} = 490 \text{ nm}$), and values at plateau were averaged after subtracting the background fluorescence of 1.5 μM ThT solution. The fluorescence intensities were compared and the % inhibition was calculated.

PAMPA assay. To predict passive blood-brain penetration of novel compounds, a modification of the parallel artificial membrane permeation assay (PAMPA) has been used based on reported protocol^{44,66}. The filter membrane of the donor plate was coated with PBL (Polar Brain Lipid, Avanti, USA) in dodecane (4 μl of 20 mg/ml PBL in dodecane) and the acceptor well was filled with 300 μl of PBS pH 7.4 buffer (V_A). Tested compounds were dissolved first in DMSO (0.5% (V/V) final) and that diluted

with PBS pH 7.4 to reach the final concentration 50 μ M in the donor well. 300 μ L of the donor solution was added to the donor wells (V_D) and the donor filter plate was carefully put on the acceptor plate so that coated membrane was “in touch” with both donor solution and acceptor buffer. Test compound diffused from the donor well through the lipid membrane (Area = 0.28 cm²) to the acceptor well. The concentration of the drug in both donor and the acceptor wells was assessed after 3, 4, 5 and 6 h of incubation in quadruplicate using the UV plate reader Synergy HT (Biotek, USA) at the maximum absorption wavelength and the standard curve for each compound. The data are presented as the permeability (Pe) according the equation (1) ^{67,68}:

$$Pe = C \times -\ln\left(1 - \frac{[drug]_{acceptor}}{[drug]_{equilibrium}}\right) \text{ where } C = \left(\frac{V_D \times V_A}{(V_D + V_A) \times Area \times Time}\right) \quad (1)$$

Table 4: Prediction of blood-brain barrier penetration of drugs expressed as Pe \pm SEM

Compound	BBB penetration estimation	
	Pe \pm SEM (*10 ⁻⁶ cm s ⁻¹)	CNS (+/-)
(+) BIGI-3h	8.2 \pm 0.37	CNS+
(-) BIGI-3h	9.7 \pm 1.6	CNS+
(\pm) BIGI-3e	3.1 \pm 0.31	CNS \pm
(\pm) BIGI-3k	1.5 \pm 0.12	CNS -
Tacrine	6.0 \pm 0.6	CNS +
Donepezil	21.9 \pm 2.1	CNS +
Rivastigmine	20.0 \pm 2.0	CNS +
Testosterone	22.7 \pm 4.3	CNS +
Chlorpromazine	9.6 \pm 1.6	CNS +
Cefuroxim	0.63 \pm 0.16	CNS -
Obidoxime	0.7 \pm 0.18	CNS -
Furosemide	0.19 \pm 0.07	CNS -

CNS (+) (high BBB permeation predicted); Pe (10⁻⁶ cm s⁻¹) > 4.0, CNS (-) (low BBB permeation predicted); Pe (10⁻⁶ cm s⁻¹) < 2.0, CNS (+/-) (BBB permeation uncertain); Pe (10⁻⁶ cm s⁻¹) from 4.0 to 2.0

In silico experimental section. From the online PDB database (www.pdb.org) model of *hAChE* (PDB ID: 4EY7, resolution: 2.35 Å) was downloaded and prepared for flexible molecular docking by MGL Tools utilities.⁴⁵ The preparation of this receptor involved removal of the surplus copies of the enzyme chains, non-bonded inhibitors, addition of polar hydrogens and merging of non-polar ones. Default Gasteiger charges were assigned to all atoms. Flexible parts of the enzymes were determined by a spherical selection of residues ($R = 11 \text{ \AA}$) approximately around the center of the active site. In the same points the centers of the grid box of $33 \times 33 \times 33 \text{ \AA}$ were positioned. The rotatable bonds in the flexible residues were detected automatically by AutoDock Tools 1.5.4 program. Given the limitation of the program used for flexible molecular docking, water molecules had to be removed from the system. Following xyz coordinate of the grid box center was applied: *hAChE* (10.698, -58.115, -23.192). The studied ligands were firstly drawn in HyperChem 8.0, then manually protonated as suggested by MarvinSketch 6.2.0. software (<http://www.chemaxon.com>), geometrically optimized by semi-empirical quantum-chemistry PM3 method and stored as pdb files. The structures of the ligands were processed for docking in a similar way as abovementioned flexible parts of the receptor by AutoDock Tools 1.5.4 program. Molecular docking was carried out in AutoDock Vina 1.1.2 program utilizing computer resources of the Czech National Grid Infrastructure MetaCentrum. The search algorithm of AutoDock Vina efficiently combines a Markov chain Monte Carlo like method for the global search and a Broyden-Fletcher-Goldfarb-Shano gradient approach for the local search.⁴⁶ It is a type of memetic algorithm based on interleaving stochastic and deterministic calculations.⁶⁹ Each docking task was repeated 30 times with the exhaustiveness parameter set to 16, employing 16 CPU in parallel multithreading. From the obtained results, the solutions reaching the minimum predicted Gibbs binding energy were taken as the top-scoring modes. The graphic representations of the docked poses were rendered in PyMOL 2.4.1 (The PyMOL Molecular Graphics System, Version 2.4.1 Schrödinger, LLC.). 2D diagrams were generated using Discovery Studio Visualizer v. 20.1.0.19295 (BIOVIA, Dassault Systèmes, Release 2019, San Diego, USA).

MAO-A & MAO-B inhibition. The inhibition assay for MAO-A and MAO-B was conducted in a white opaque 96-well microplate. The reaction mixture contains 42 nM MAO-A or 200 nM MAO-B and

inhibitors (+) **BIGI-3h** and (-) **BIGI-3h** in final concentrations ranging from 0.1-200 μM in 50 mM potassium phosphate buffer with 20% (v/v) glycerol (pH 7.5). The mixture was pre-incubated at 37 °C for 15 min and subsequently substrate kynuramine was added to the final concentration of 50 μM . The whole reaction mixture was incubated at 37°C for 30 min. The deamination product of kynuramine formed during the enzymatic reaction (4-hydroxyquinoline) was determined by fluorescence detection (ex 310/em 400 nm) using microplate reader (Spark multimode microplate reader, Tecan Group Ltd). IC_{50} values were calculated by adjusting the experimental data (enzyme activity versus concentration of inhibitor) to non-linear regression curves using GraphPad Prism 7.

The determination of K_i values was performed for MAO-B enzyme with three different concentrations of each inhibitor: 5 μM , 15 μM and 50 μM . The final concentrations of these inhibitors in the reaction mixture were proposed to cover the entire inhibitory range.

GSK-3 β inhibition in vitro assay. Human recombinant GSK-3 β , prephosphorylated polypeptide substrate and white 96-well plates were purchased from Millipore (Millipore Iberica S.A.U.). Kinase-Glo Luminescent Kinase Assay was obtained from Promega (Promega Biotech Iberica, SL). Adenosinetriphosphate (ATP) and all other reagents were from Sigma-Aldrich. Assay buffer contained 50 mM 4-(2-hydroxyethyl)-1-piperazineethanesulfonic acid (HEPES) (pH 7.5), 1 mM ethylenediaminetetraacetic acid (EDTA), 1 mM ethylene glycol tetraacetic acid (EGTA), and 15 mM magnesium acetate. The in solution experiments for GSK-3 β inhibition analysis were performed by following the method developed by Baki et al⁵³. In a typical assay, 10 μL of test compound (dissolved in DMSO at 1 mM concentration and diluted in advance in assay buffer to the desired concentration) and 10 μL (20 ng) of enzyme were added to each well in presence of 20 μL of assay buffer containing GSM substrate and ATP in order to reach a 25 μM and 1 μM final concentration respectively. The final DMSO percentage in the reaction mixture did not exceed 5%. After a 30 min incubation time at 30 °C, the enzymatic reaction was stopped by adding 40 μL of Kinase-Glo reagent. Glow-type luminescence was recorded after 10 min using a VictorX 3 PerkinElmer plate reader. The activity was found proportional to the difference of the total and consumed ATP. The inhibitory activities were calculated on the basis of maximal kinase (average positive) and luciferase activities (average negative) measured

in the absence of inhibitor and in the presence of reference compound inhibitor (SB-415286 Merck Millipore, $IC_{50} = 55$ nM) at total inhibition concentration ($5 \mu\text{M}$)⁷⁰, respectively. The linear regression parameters were determined and the IC_{50} extrapolated (GraphPad Prism 4.0, GraphPad Software Inc.).

Tau(306-336) peptide aggregation and its inhibition by ThT fluorimetric assay. 1 mg of Tau(306-336) (Bachem AG, Germany) was initially dissolved in 1,1,1,3,3,3-hexafluoro-2-propanol (HFIP), gently vortexed, sonicated, and kept overnight at room temperature. Subsequently, the sample was aliquoted dried and stored at -20 °C.

Stock solutions of Tau(306-336) peptide ($500 \mu\text{M}$) were prepared in ultrapure water and immediately used. Stock solution of thioflavin T (ThT, $500 \mu\text{M}$) was prepared in 56.3 mM phosphate buffer (PB, pH = 7.4) while stock solution of inhibitors and doxycycline (20 mM) were prepared in DMSO/methanol 10/90. Tau(306-336) aggregation was monitored at 30 °C in black, clear bottom 96-well plate (Greiner) by EnSpire multi-plate reader (Perkin Elmer) using ThT fluorimetric assay⁶ with some variations. The excitation and emission wavelengths were set at 446 and 490 nm, respectively. Assay samples were prepared by diluting Tau(306-336) stock solution to $50 \mu\text{M}$ in the assay mixture which consisted in $20 \mu\text{M}$ ThT, 48.1 mM PB (final concentrations) in final $100 \mu\text{L}$ volume (final DMSO and MeOH content: 0.05% and 0.45% , respectively). Inhibition experiments were performed by incubating Tau(306-336) peptide at the given conditions in the presence of tested inhibitors at $50 \mu\text{M}$. Fluorescence data were recorded every 10 min overnight with 1 min shaking at 800 rpm prior to each reading. Each inhibitor was assayed in triplicates in at least two independent experiments. Estimation of the inhibitory potency (%) was carried out by comparing fluorescence values at the plateau (average fluorescence intensity value in the $12 - 16$ h range). % Inhibition is expressed as the mean \pm SEM. Quenching of ThT fluorescence was evaluated by preparing blank solutions containing inhibitor/reference compound and preformed fibrils of Tau(306-336) peptide.

In vivo test. For behavioural studies, we used 50 swiss female 10 -week-old mice weighing $25-30$ g. Memory impairment was induced by the potent antimuscarinic drug scopolamine hydrobromide (1 mg/kg, Sigma) dissolved in saline buffer. To explore the potential of (\pm) **BIGI-3h** as a cognitive

enhancer, we administered the hybrid drug at a dose of 1 mg/kg and 10 mg/kg. We tested the anti-amnesic effect of donepezil (Tocris Bioscience, R&D Systems Inc.) at a dose of 1 mg/kg. Both products, (\pm) **BIGI-3h** and donepezil, were dissolved in saline buffer containing 3.6% DMSO. All drug solutions were independently prepared immediately before their use and were administered intraperitoneally in 10 mL/kg of vehicle volume. Different batches of mice were used for each experiment. The animals were distributed into 5 experimental groups (I–V): control groups (I) mice administered 3.6% DMSO in saline buffer, labelled as “control vehicle”; experimental groups (II–V) consisted of (II) mice administered scopolamine dissolved in 3.6% DMSO in saline buffer, labelled as “scopo/DMSO,” (III) mice coadministered scopolamine plus Donepezil, labelled as “Scopo/donep,” (IV) and (V) mice coadministered scopolamine plus (\pm) **BIGI-3h** at 1mg/Kg and 10mg/Kg labelled respectively “Scopo/**BIGI-3h** 1” “Scopo/**BIGI-3h** 10”.

Object Recognition task. Spontaneous object recognition was tested as described previously⁵⁶ with slight modifications. All behavioural experiments took place during the light phase of the 12-h light/dark cycle between 10 am and 3 pm to minimize the influence of circadian rhythm. The ORT was performed in a round plastic open field (diameter: 48cm) with black walls (40 cm high). The apparatus was placed in a poorly illuminated (60 lux) and noise-isolated room, and the mice were randomly placed in the experimental room 1 hour before beginning the experimental task each day. The behaviour of the animals (time spent exploring the objects and overall locomotor activity) was registered during precise time periods. On the first day animals were allowed to explore the apparatus individually for 5 min in the absence of objects (habituation session). On the second day, 30 min before the trial session, mice were administered treatments as indicated in the previous section and then subjected to the acquisition trial (T1). Mice were individually allowed for 5 min to freely explore 2 identical plastic objects placed in the arena, located in symmetric positions at a distance of about 7 cm away from walls. Then the rodents were removed from the open field for an interval of 1 hour. After this delay, we performed the retention trial (T2). Animals were returned for 5 min to the bin where 1 of the original objects had been replaced by a novel object (neutral to naive mice) with a different shape, color and textures than the remaining object previously presented in the acquisition trial (familiar object). To score the exploration behavior

of the mice, a camera was mounted above the center of the arena. The total time spent in active exploration of each object during T2 was determined through analyzation of the video recording. As a criterion of active object exploration, we measured the time spent by the animal directing its nose to the object at a distance of less than 2 cm and/or touching it with the vibrissae or nose and/or climbing on it. The recognition index was calculated as following: time spent exploring the novel object/ (time spent exploring the novel object+time exploring the familiar object). Statistical analyses were performed using the X² test. We used the Bonferroni correction for multiple comparisons. We considered differences to be significant at p<0.05. Results are presented as mean and standard error.

All animal experiments comply with the ARRIVE (Animal Research: Reporting of In Vivo Experiments) guidelines and are carried out in accordance with the EU Directive 2010/63/EU for the care and the use of laboratory animals. The protocol were approved by the Franche-Comté University's Animal Care Committee (protol number: 2015-004-EH-12PR)

ASSOCIATED CONTENT

Supporting Information

¹H NMR and ¹³C NMR spectra for key compounds (PDF)

The Supporting Information is available free of charge at <https://pubs.acs.org>.

AUTHOR INFORMATION

Corresponding Author

Lhassane Ismaili, phone +33381665543 Email : lhassane.ismaili@univ-fcomte.fr

Neurosciences intégratives et cliniques EA 481, Univ. Bourgogne Franche-Comté, F-25000 Besançon, France.

Authors

Julie Monnin, Neurosciences intégratives et cliniques EA 481, Univ. Bourgogne Franche-Comté, F-25000 Besançon, France.

Adeline Etievant, Neurosciences intégratives et cliniques EA 481, Univ. Bourgogne Franche-Comté, F-25000 Besançon, France.

Raquel L. Arribas, Servicio de Farmacología Clínica, Instituto de Investigación Sanitaria, Hospital Universitario de la Princesa, C/ Diego de León, 62, 28006 Madrid (Spain) and Instituto Teofilo Hernando, Universidad Autónoma de Madrid, C/ Arzobispo Morcillo, 4, 28029 Madrid (Spain)

Lucía Viejo, Servicio de Farmacología Clínica, Instituto de Investigación Sanitaria, Hospital Universitario de la Princesa, C/ Diego de León, 62, 28006 Madrid (Spain) and Instituto Teofilo Hernando, Universidad Autónoma de Madrid, C/ Arzobispo Morcillo, 4, 28029 Madrid (Spain)

Bernard Refouvelet, Neurosciences intégratives et cliniques EA 481, Univ. Bourgogne Franche-Comté, F-25000 Besançon, France.

Ondrej Soukup, Biomedical Research Center, University Hospital Hradec Kralove, Czech Republic, University of Defence, Hradec Kralove, (Czech Republic)

Jana Janockova, Biomedical Research Center, University Hospital Hradec Kralove, Czech Republic, University of Defence, Hradec Kralove, (Czech Republic)

Vendula Hepnarova, Department of Toxicology and Military Pharmacy, Faculty of Military Health Sciences (Czech Republic)

Jan Korabecny, Biomedical Research Center, University Hospital Hradec Kralove, Czech Republic, University of Defence, Hradec Kralove, (Czech Republic)

Tomas Kucera, Department of Toxicology and Military Pharmacy, Faculty of Military Health Sciences (Czech Republic)

Daniel Jun, Department of Toxicology and Military Pharmacy, Faculty of Military Health Sciences (Czech Republic)

Rudolf Andrys, University Hradec Kralove, Faculty of Science, Department of Chemistry, Rokitanskeho 62, 50003 Hradec Kralove, (Czech Republic)

Kamil Musilek, University Hradec Kralove, Faculty of Science, Department of Chemistry, Rokitanskeho 62, 50003 Hradec Kralove, (Czech Republic)

Aurelie Baguet, Université Bourgogne Franche Comté, France, INSERM, UMR1098, Interactions Hôte-Greffon-Tumeur/Ingénierie Cellulaire et Génique, F-25000, Besançon, (France).

Eva M García-Frutos, Instituto de Ciencia de Materiales de Madrid, CSIC, Cantoblanco 28049, Madrid (Spain)

Angela De Simone, Department for Life Quality Studies University of Bologna Corso di Augusto, 237, 47921-Rimini, (Italy)

Vincenza Andrisano, Department for Life Quality Studies University of Bologna Corso di Augusto, 237, 47921-Rimini, (Italy)

Manuela Bartolini, Department of Pharmacy and Biotechnology Alma Mater Studiorum—University of Bologna Via Belmeloro 6, 40126-Bologna, (Italy)

Cristóbal de los Ríos, Servicio de Farmacología Clínica, Instituto de Investigación Sanitaria, Hospital Universitario de la Princesa, C/ Diego de León, 62, 28006 Madrid (Spain) and Instituto Teofilo Hernando, Universidad Autónoma de Madrid, C/ Arzobispo Morcillo, 4, 28029 Madrid (Spain)

José Marco-Contelles, Laboratory of Medicinal Chemistry (IQOG, CSIC), Juan de la Cierva 3; 28006-Madrid, Spain

Emmanuel Haffen, Neurosciences intégratives et cliniques EA 481, Univ. Bourgogne Franche-Comté, F-25000 Besançon, France

Author Contributions

LI conceived, designed, synthesized compounds, determined ORAC values and supervised the whole project, JM and AE designed and carried out the in vivo NOR studies, EH (lead), R-L-A, LV carried out the calcium channel study, CdIR (lead), JJ, VH, TK carried out the PAMPA, Cholinesterases inhibition OS and DJ (leads), JJ performed the molecular docking studies, RA did the MAO inhibition KM (lead), AB did alkaline phosphatase experiment, LI, Br, EM G-F writing of original draft, AdS, VA and MB designed and performed Abeta and tau self-aggregation and GSK3 β inhibition, JM-C supervised biological evaluation and chiral separation. The manuscript was revised and approved by all authors.

Conflict of Interest

Author LI declares a conflict of interest based on a related patent application. The other authors declare no conflicts of interest.

FUNDING AND ACKNOWLEDGMENT

LI thanks the Regional Council of Franche-Comté (2016YC-04540 and 04560) for financial support; Mrs. M.-J. Henriot (PHV Pharma) for her support in the HPLC analyses, Vincent luzet for preliminary results in synthesis. OS, JJ and JK acknowledge the support from MH CZ - DRO (University Hospital Hradec Kralove, Nr. 00179906). TK, DJ, and VH acknowledge support from the Long-term Development Plan (Faculty of Military Health Sciences). R.A. and K.M. thanks Ministry of Education, Youth and Sports of the Czech Republic (ERDF no. CZ.02.1.01/0.0/0.0/16_025/0007444) and University of Hradec Kralove (no. VT2019-2021)

REFERENCES

- (1) Cacabelos, R. Have There Been Improvements in Alzheimer's Disease Drug Discovery over the Past 5 Years? *Expert Opin. Drug Discov.* **2018**, *13* (6), 523–538. <https://doi.org/10.1080/17460441.2018.1457645>.
- (2) Querfurth, H. W.; LaFerla, F. M. Alzheimer's Disease. *N. Engl. J. Med.* **2010**, *362* (4), 329–344. <https://doi.org/10.1056/NEJMra0909142>.
- (3) Bartus, R. T.; Dean, R. L.; Beer, B.; Lippa, A. S. The Cholinergic Hypothesis of Geriatric Memory Dysfunction. *Science* **1982**, *217* (4558), 408–414.
- (4) Hamley, I. W. The Amyloid Beta Peptide: A Chemist's Perspective. Role in Alzheimer's and Fibrillization. *Chem. Rev.* **2012**, *112* (10), 5147–5192. <https://doi.org/10.1021/cr3000994>.
- (5) Liu, M.; Dexheimer, T.; Sui, D.; Hovde, S.; Deng, X.; Kwok, R.; Bochar, D. A.; Kuo, M.-H. Hyperphosphorylated Tau Aggregation and Cytotoxicity Modulators Screen Identified Prescription Drugs Linked to Alzheimer's Disease and Cognitive Functions. *Sci. Rep.* **2020**, *10* (1), 16551. <https://doi.org/10.1038/s41598-020-73680-2>.
- (6) Gandini, A.; Bartolini, M.; Tedesco, D.; Martinez-Gonzalez, L.; Roca, C.; Campillo, N. E.; Zaldivar-Diez, J.; Perez, C.; Zuccheri, G.; Miti, A.; Feoli, A. et al. Tau-Centric Multitarget Approach for Alzheimer's Disease: Development of First-in-Class Dual Glycogen Synthase Kinase 3 β and Tau-Aggregation Inhibitors. *J Med Chem* **2018**, *61* (17), 7640–7656. <https://doi.org/10.1021/acs.jmedchem.8b00610>.
- (7) Gómez-Isla, T.; Hollister, R.; West, H.; Mui, S.; Growdon, J. H.; Petersen, R. C.; Parisi, J. E.; Hyman, B. T. Neuronal Loss Correlates with but Exceeds Neurofibrillary Tangles in Alzheimer's Disease. *Ann. Neurol.* **1997**, *41* (1), 17–24. <https://doi.org/10.1002/ana.410410106>.
- (8) Masters, C. L.; Bateman, R.; Blennow, K.; Rowe, C. C.; Sperling, R. A.; Cummings, J. L. Alzheimer's Disease. *Nat. Rev. Dis. Primers* **2015**, *1* (1), 1–18. <https://doi.org/10.1038/nrdp.2015.56>.
- (9) Chen, C.-H.; Zhou, W.; Liu, S.; Deng, Y.; Cai, F.; Tone, M.; Tone, Y.; Tong, Y.; Song, W. Increased NF- κ B Signalling up-Regulates BACE1 Expression and Its Therapeutic Potential in Alzheimer's Disease. *Int. J. Neuropsychopharmacol.* **2012**, *15* (1), 77–90. <https://doi.org/10.1017/S1461145711000149>.
- (10) Oulès, B.; Del Prete, D.; Greco, B.; Zhang, X.; Lauritzen, I.; Sevalle, J.; Moreno, S.; Paterlini-Bréchet, P.; Trebak, M.; Checler, et al. Ryanodine Receptor Blockade Reduces Amyloid- β Load and Memory Impairments in Tg2576 Mouse Model of Alzheimer Disease. *J.*

- Neurosci.* **2012**, *32* (34), 11820–11834. <https://doi.org/10.1523/JNEUROSCI.0875-12.2012>.
- (11) Avila, J.; Pérez, M.; Lim, F.; Gómez-Ramos, A.; Hernández, F.; Lucas, J. J. Tau in Neurodegenerative Diseases: Tau Phosphorylation and Assembly. *neurotox res* **2004**, *6* (6), 477–482. <https://doi.org/10.1007/BF03033284>.
- (12) Chakraborty, S.; Stutzmann, G. E. Calcium Channelopathies and Alzheimer's Disease: Insight into Therapeutic Success and Failures. *Eur. J. Pharmacol* **2014**, *739*, 83–95. <https://doi.org/10.1016/j.ejphar.2013.11.012>.
- (13) L'Episcopo, F.; Drouin-Ouellet, J.; Tirolo, C.; Pulvirenti, A.; Giugno, R.; Testa, N.; Caniglia, S.; Serapide, M. F.; Cisbani, G.; Barker, R. A.; et al. GSK-3 β -Induced Tau Pathology Drives Hippocampal Neuronal Cell Death in Huntington's Disease: Involvement of Astrocyte-Neuron Interactions. *Cell Death Dis* **2016**, *7*, e2206. <https://doi.org/10.1038/cddis.2016.104>.
- (14) Beurel, E.; Grieco, S. F.; Jope, R. S. Glycogen Synthase Kinase-3 (GSK3): Regulation, Actions, and Diseases. *Pharmacol Ther* **2015**, *0*, 114–131. <https://doi.org/10.1016/j.pharmthera.2014.11.016>.
- (15) Maqbool, M.; Mobashir, M.; Hoda, N. Pivotal Role of Glycogen Synthase Kinase-3: A Therapeutic Target for Alzheimer's Disease. *Eur. J. Med. Chem.* **2016**, *107*, 63–81. <https://doi.org/10.1016/j.ejmech.2015.10.018>.
- (16) Yan, M. H.; Wang, X.; Zhu, X. Mitochondrial Defects and Oxidative Stress in Alzheimer Disease and Parkinson Disease. *Free Radic. Biol. Med.* **2013**, *62*, 90–101. <https://doi.org/10.1016/j.freeradbiomed.2012.11.014>.
- (17) Greenough, M. A.; Camakaris, J.; Bush, A. I. Metal Dyshomeostasis and Oxidative Stress in Alzheimer's Disease. *Neurochem. Int.* **2013**, *62* (5), 540–555. <https://doi.org/10.1016/j.neuint.2012.08.014>.
- (18) Candore, G.; Bulati, M.; Caruso, C.; Castiglia, L.; Colonna-Romano, G.; Di Bona, D.; Duro, G.; Lio, D.; Matranga, D.; Pellicanò, M.; et al. Inflammation, Cytokines, Immune Response, Apolipoprotein E, Cholesterol, and Oxidative Stress in Alzheimer Disease: Therapeutic Implications. *Rejuvenation Res* **2010**, *13* (2–3), 301–313. <https://doi.org/10.1089/rej.2009.0993>.
- (19) Rosini, M.; Simoni, E.; Milelli, A.; Minarini, A.; Melchiorre, C. Oxidative Stress in Alzheimer's Disease: Are We Connecting the Dots? *J. Med. Chem.* **2014**, *57* (7), 2821–2831. <https://doi.org/10.1021/jm400970m>.
- (20) Reis, J.; Cagide, F.; Valencia, M. E.; Teixeira, J.; Bagetta, D.; Pérez, C.; Uriarte, E.; Oliveira, P. J.; Ortuso, F.; Alcaro, S.; et al. F. Multi-Target-Directed Ligands for Alzheimer's Disease: Discovery of Chromone-Based Monoamine Oxidase/Cholinesterase Inhibitors. *Eur. J. Med. Chem* **2018**, *158*, 781–800. <https://doi.org/10.1016/j.ejmech.2018.07.056>.
- (21) Albertini, C.; Salerno, A.; Pinheiro, P. de S. M.; Bolognesi, M. L. From Combinations to Multitarget-Directed Ligands: A Continuum in Alzheimer's Disease Polypharmacology. *Medicinal Research Reviews n/a* (n/a). <https://doi.org/10.1002/med.21699>.
- (22) Prati, F.; Cavalli, A.; Bolognesi, M. L. Navigating the Chemical Space of Multitarget-Directed Ligands: From Hybrids to Fragments in Alzheimer's Disease. *Molecules* **2016**, *21* (4), 466. <https://doi.org/10.3390/molecules21040466>.
- (23) Guzior, N.; Wi.eckowska, A.; Panek, D.; Malawska, B. Recent Development of Multifunctional Agents as Potential Drug Candidates for the Treatment of Alzheimer's Disease. *CMC* **2014**, *22* (3), 373–404. <https://doi.org/10.2174/0929867321666141106122628>.
- (24) Malek, R.; Arribas, R. L.; Palomino-Antolin, A.; Totoson, P.; Demougeot, C.; Kobrlova, T.; Soukup, O.; Iriepa, I.; Moraleda, I.; Diez-Iriepa, D.; et al. New Dual Small Molecules for Alzheimer's Disease Therapy Combining Histamine H3 Receptor (H3R) Antagonism and Calcium Channels Blockade with Additional Cholinesterase Inhibition. *J. Med. Chem.* **2019**, *62* (24), 11416–11422. <https://doi.org/10.1021/acs.jmedchem.9b00937>.

- (25) Dömling, A.; Wang, W.; Wang, K. Chemistry and Biology Of Multicomponent Reactions. *Chem. Rev.* **2012**, *112* (6), 3083–3135. <https://doi.org/10.1021/cr100233r>.
- (26) Akritopoulou-Zanze, I. Isocyanide-Based Multicomponent Reactions in Drug Discovery. *Curr Opin Chem Biol* **2008**, *12* (3), 324–331. <https://doi.org/10.1016/j.cbpa.2008.02.004>.
- (27) Ismaili, L.; do Carmo Carreiras, M. Multicomponent Reactions for Multitargeted Compounds for Alzheimer's Disease. *Curr. Top. Med. Chem.* **2018**, *17* (31), 3319–3327. <https://doi.org/10.2174/1568026618666180112155424>.
- (28) Benchekroun, M.; Ismaili, L.; Pudlo, M.; Luzet, V.; Gharbi, T.; Refouvelet, B.; Marco-Contelles, J. Donepezil–Ferulic Acid Hybrids as Anti-Alzheimer Drugs. *Future Med Chem* **2015**, *7* (1), 15–21. <https://doi.org/10.4155/fmc.14.148>.
- (29) Benchekroun, M.; Romero, A.; Egea, J.; León, R.; Michalska, P.; Buendía, I.; Jimeno, M. L.; Jun, D.; Janockova, J.; Sepsova, V.; et al. The Antioxidant Additive Approach for Alzheimer's Disease Therapy: New Ferulic (Lipoic) Acid Plus Melatonin Modified Tacrines as Cholinesterases Inhibitors, Direct Antioxidants, and Nuclear Factor (Erythroid-Derived 2)-Like 2 Activators. *J. Med. Chem.* **2016**, *59* (21), 9967–9973. <https://doi.org/10.1021/acs.jmedchem.6b01178>.
- (30) Malek, R.; Maj, M.; Wnorowski, A.; Jóźwiak, K.; Martin, H.; Iriepa, I.; Moraleda, I.; Chabchoub, F.; Marco-Contelles, J.; Ismaili, L. Multi-Target 1,4-Dihydropyridines Showing Calcium Channel Blockade and Antioxidant Capacity for Alzheimer's Disease Therapy. *Bioorg. Chem.* **2019**, *91*, 103205. <https://doi.org/10.1016/j.bioorg.2019.103205>.
- (31) Jalili-Baleh, L.; Babaei, E.; Abdpour, S.; Nasir Abbas Bukhari, S.; Foroumadi, A.; Ramazani, A.; Sharifzadeh, M.; Abdollahi, M.; Khoobi, M. A Review on Flavonoid-Based Scaffolds as Multi-Target-Directed Ligands (MTDLs) for Alzheimer's Disease. *Eur.J. Med. Chem.* **2018**, *152*, 570–589. <https://doi.org/10.1016/j.ejmech.2018.05.004>.
- (32) Matos, L. H. S.; Masson, F. T.; Simeoni, L. A.; Homem-de-Mello, M. Biological Activity of Dihydropyrimidinone (DHPM) Derivatives: A Systematic Review. *Eur.J. Med. Chem* **2018**, *143*, 1779–1789. <https://doi.org/10.1016/j.ejmech.2017.10.073>.
- (33) Grover, G. J.; Dzwonczyk, S.; McMullen, D. M.; Normandin, D. E.; Parham, C. S.; Sleph, P. G.; Moreland, S. Pharmacologic Profile of the Dihydropyrimidine Calcium Channel Blockers SQ 32,547 and SQ 32,926 [Correction of SQ 32,946]. *J. Cardiovasc. Pharmacol.* **1995**, *26* (2), 289–294. <https://doi.org/10.1097/00005344-199508000-00015>.
- (34) Cohen, P.; Goedert, M. GSK3 Inhibitors: Development and Therapeutic Potential. *Nat. Rev. Drug. Discov.* **2004**, *3* (6), 479–487. <https://doi.org/10.1038/nrd1415>.
- (35) Prati, F.; De Simone, A.; Bisignano, P.; Armirotti, A.; Summa, M.; Pizzirani, D.; Scarpelli, R.; Perez, D. I.; Andrisano, V.; Perez-Castillo, A.; et al. Multitarget Drug Discovery for Alzheimer's Disease: Triazinones as BACE-1 and GSK-3 β Inhibitors. *Angew. Chem. Int. Ed.* **2015**, *54* (5), 1578–1582. <https://doi.org/10.1002/anie.201410456>.
- (36) Choi, J. Y.; Calvet, C. M.; Gunatilleke, S. S.; Ruiz, C.; Cameron, M. D.; McKerrow, J. H.; Podust, L. M.; Roush, W. R. Rational Development of 4-Aminopyridyl-Based Inhibitors Targeting Trypanosoma Cruzi CYP51 as Anti-Chagas Agents. *J. Med. Chem.* **2013**, *56* (19), 7651–7668. <https://doi.org/10.1021/jm401067s>.
- (37) Carling, W. R.; Moore, K. W. Imidazolone and Oxazolone Derivatives as Dopamine Antagonists. US5698573A, December 16, 1997.
- (38) Ellman, G. L.; Courtney, K. D.; Andres jr., V.; Featherstone, R. M. A New and Rapid Colorimetric Determination of Acetylcholinesterase Activity. *Biochem. Pharmacol.* **1961**, *7* (2), 88–95. [https://doi.org/10.1016/0006-2952\(61\)90145-9](https://doi.org/10.1016/0006-2952(61)90145-9).
- (39) Pachón-Angona, I.; Refouvelet, B.; Andrés, R.; Martin, H.; Luzet, V.; Iriepa, I.; Moraleda, I.; Diez-Iriepa, D.; Oset-Gasque, M.-J.; Marco-Contelles, et al. Donepezil + Chromone + Melatonin Hybrids as Promising Agents for Alzheimer's Disease

- Therapy. *J Enzyme Inhib Med Chem* **2019**, *34* (1), 479–489.
<https://doi.org/10.1080/14756366.2018.1545766>.
- (40) Benchekroun, M; Bartolini, M; Egea, J; Romero, A; Soriano, E; Pudlo, M; Luzet, V; Andrisano, V; Jimeno, ML; Lopez, MG; et al. Novel Tacrine-Grafted Ugi Adducts as Multipotent Anti-Alzheimer Drugs: A Synthetic Renewal in Tacrine-Ferulic Acid Hybrids *ChemMedChem*: **2015**, *10* (3), 523-539. <https://doi.org/10.1002/cmdc.201402409>.
- (41) Ou, B.; Hampsch-Woodill, M.; Prior, R. L. Development and Validation of an Improved Oxygen Radical Absorbance Capacity Assay Using Fluorescein as the Fluorescent Probe. *J. Agric. Food Chem.* **2001**, *49* (10), 4619–4626.
- (42) Dávalos, A.; Gómez-Cordovés, C.; Bartolomé, B. Extending Applicability of the Oxygen Radical Absorbance Capacity (ORAC-Fluorescein) Assay. *J. Agric. Food Chem.* **2004**, *52* (1), 48–54. <https://doi.org/10.1021/jf0305231>.
- (43) Bartolini, M.; Bertucci, C.; Bolognesi, M. L.; Cavalli, A.; Melchiorre, C.; Andrisano, V. Insight into the Kinetic of Amyloid Beta (1-42) Peptide Self-Aggregation: Elucidation of Inhibitors' Mechanism of Action. *ChemBioChem* **2007**, *8* (17), 2152–2161.
<https://doi.org/10.1002/cbic.200700427>.
- (44) Di, L.; Kerns, E. H.; Fan, K.; McConnell, O. J.; Carter, G. T. High Throughput Artificial Membrane Permeability Assay for Blood–Brain Barrier. *Eur. J. Med. Chem.* **2003**, *38* (3), 223–232. [https://doi.org/10.1016/S0223-5234\(03\)00012-6](https://doi.org/10.1016/S0223-5234(03)00012-6).
- (45) Cheung, J.; Rudolph, M. J.; Burshteyn, F.; Cassidy, M. S.; Gary, E. N.; Love, J.; Franklin, M. C.; Height, J. J. Structures of Human Acetylcholinesterase in Complex with Pharmacologically Important Ligands. *J. Med. Chem.* **2012**, *55* (22), 10282–10286.
<https://doi.org/10.1021/jm300871x>.
- (46) Trott, O.; Olson, A. J. AutoDock Vina: Improving the Speed and Accuracy of Docking with a New Scoring Function, Efficient Optimization, and Multithreading. *J Comput Chem* **2010**, *31* (2), 455–461. <https://doi.org/10.1002/jcc.21334>.
- (47) Spilovska, K.; Korabecny, J.; Sepsova, V.; Jun, D.; Hrabnova, M.; Jost, P.; Muckova, L.; Soukup, O.; Janockova, J.; Kucera, T.; et al. Novel Tacrine-Scutellarin Hybrids as Multipotent Anti-Alzheimer's Agents: Design, Synthesis and Biological Evaluation. *Molecules* **2017**, *22* (6), 1006. <https://doi.org/10.3390/molecules22061006>.
- (48) Korabecny, J.; Andrs, M.; Nepovimova, E.; Dolezal, R.; Babkova, K.; Horova, A.; Malinak, D.; Mezeiova, E.; Gorecki, L.; Sepsova, V.; et al. 7-Methoxytacrine-p-Anisidine Hybrids as Novel Dual Binding Site Acetylcholinesterase Inhibitors for Alzheimer's Disease Treatment. *Molecules* **2015**, *20* (12), 22084–22101.
<https://doi.org/10.3390/molecules201219836>.
- (49) Nepovimova, E.; Korabecny, J.; Dolezal, R.; Babkova, K.; Ondrejicek, A.; Jun, D.; Sepsova, V.; Horova, A.; Hrabnova, M.; Soukup, O.; et al. Tacrine–Trolox Hybrids: A Novel Class of Centrally Active, Nonhepatotoxic Multi-Target-Directed Ligands Exerting Anticholinesterase and Antioxidant Activities with Low In Vivo Toxicity. *J. Med. Chem.* **2015**, *58* (22), 8985–9003. <https://doi.org/10.1021/acs.jmedchem.5b01325>.
- (50) Zemek, F.; Drtinova, L.; Nepovimova, E.; Sepsova, V.; Korabecny, J.; Klimes, J.; Kuca, K. Outcomes of Alzheimer's Disease Therapy with Acetylcholinesterase Inhibitors and Memantine. *Expert Opin Drug Saf* **2014**, *13* (6), 759–774.
<https://doi.org/10.1517/14740338.2014.914168>.
- (51) Inestrosa, N. C.; Alvarez, A.; Pérez, C. A.; Moreno, R. D.; Vicente, M.; Linker, C.; Casanueva, O. I.; Soto, C.; Garrido, J. Acetylcholinesterase Accelerates Assembly of Amyloid- β -Peptides into Alzheimer's Fibrils: Possible Role of the Peripheral Site of the Enzyme. *Neuron* **1996**, *16* (4), 881–891. [https://doi.org/10.1016/S0896-6273\(00\)80108-7](https://doi.org/10.1016/S0896-6273(00)80108-7).
- (52) Yan, Z.; Caldwell, G. W.; Zhao, B.; Reitz, A. B. A High-Throughput Monoamine Oxidase Inhibition Assay Using Liquid Chromatography with Tandem Mass Spectrometry.

- Rapid Commun Mass Spectrometry* **2004**, *18* (8), 834–840.
- (53) Baki, A.; Bielik, A.; Molnár, L.; Szendrei, G.; Keserü, G. M. A High Throughput Luminescent Assay for Glycogen Synthase Kinase-3beta Inhibitors. *Assay Drug Dev Technol* **2007**, *5* (1), 75–83. <https://doi.org/10.1089/adt.2006.029>.
- (54) Bergen, M. von; Friedhoff, P.; Biernat, J.; Heberle, J.; Mandelkow, E.-M.; Mandelkow, E. Assembly of τ Protein into Alzheimer Paired Helical Filaments Depends on a Local Sequence Motif (306VQIVYK311) Forming β Structure. *PNAS* **2000**, *97* (10), 5129–5134. <https://doi.org/10.1073/pnas.97.10.5129>.
- (55) Stöhr, J.; Wu, H.; Nick, M.; Wu, Y.; Bhate, M.; Condello, C.; Johnson, N.; Rodgers, J.; Lemmin, T.; Achyraya, S.; et al. 31-Residue Peptide Induces Aggregation of Tau's Microtubule-Binding Region in Cells. *Nat Chem* **2017**, *9* (9), 874–881. <https://doi.org/10.1038/nchem.2754>.
- (56) Antunes, M.; Biala, G. The Novel Object Recognition Memory: Neurobiology, Test Procedure, and Its Modifications. *Cogn Process* **2012**, *13* (2), 93–110. <https://doi.org/10.1007/s10339-011-0430-z>.
- (57) Baell, J. B.; Holloway, G. A. New Substructure Filters for Removal of Pan Assay Interference Compounds (PAINS) from Screening Libraries and for Their Exclusion in Bioassays. *J. Med. Chem.* **2010**, *53* (7), 2719–2740. <https://doi.org/10.1021/jm901137j>.
- (58) Capuzzi, S. J.; Muratov, E. N.; Tropsha, A. Phantom PAINS: Problems with the Utility of Alerts for Pan-Assay Interference CompoundS. *J Chem Inf Model* **2017**, *57* (3), 417–427. <https://doi.org/10.1021/acs.jcim.6b00465>.
- (59) Jasial, S.; Hu, Y.; Bajorath, J. How Frequently Are Pan-Assay Interference Compounds Active? Large-Scale Analysis of Screening Data Reveals Diverse Activity Profiles, Low Global Hit Frequency, and Many Consistently Inactive Compounds. *J. Med. Chem.* **2017**, *60* (9), 3879–3886. <https://doi.org/10.1021/acs.jmedchem.7b00154>.
- (60) Baell, J. B.; Nissink, J. W. M. Seven Year Itch: Pan-Assay Interference Compounds (PAINS) in 2017—Utility and Limitations. *ACS Chem. Biol.* **2018**, *13* (1), 36–44. <https://doi.org/10.1021/acscchembio.7b00903>.
- (61) Ferreira, R. S.; Simeonov, A.; Jadhav, A.; Eidam, O.; Mott, B. T.; Keiser, M. J.; McKerrow, J. H.; Maloney, D. J.; Irwin, J. J.; Shoichet, B. K. Complementarity between a Docking and a High-Throughput Screen in Discovering New Cruzain Inhibitors. *J. Med. Chem.* **2010**, *53* (13), 4891–4905. <https://doi.org/10.1021/jm100488w>.
- (62) Werner, S.; Turner, D. M.; Lyon, M. A.; Huryn, D. M.; Wipf, P. A Focused Library of Tetrahydropyrimidinone Amides via a Tandem Biginelli-Ugi Multi-Component Process. *Synlett* **2006**, *2006* (14), 2334–2338. <https://doi.org/10.1055/s-2006-949648>.
- (63) Gonzalez, D.; Arribas, R. L.; Viejo, L.; Lajarin-Cuesta, R.; de los Rios, C. Substituent Effect of N-Benzylated Gramine Derivatives That Prevent the PP2A Inhibition and Dissipate the Neuronal Ca²⁺ Overload, as a Multitarget Strategy for the Treatment of Alzheimer's Disease. *Bioorg. Med. Chem.* **2018**, *26* (9), 2551–2560. <https://doi.org/10.1016/j.bmc.2018.04.019>.
- (64) Naiki, H.; Higuchi, K.; Hosokawa, M.; Takeda, T. Fluorometric Determination of Amyloid Fibrils in Vitro Using the Fluorescent Dye, Thioflavin T1. *Anal. Biochem.* **1989**, *177* (2), 244–249.
- (65) LeVine, H. 3rd. Thioflavine T Interaction with Synthetic Alzheimer's Disease Beta-Amyloid Peptides: Detection of Amyloid Aggregation in Solution. *Protein Sci.* **1993**, *2* (3), 404–410. <https://doi.org/10.1002/pro.5560020312>.
- (66) Lemes, L. F. N.; de Andrade Ramos, G.; de Oliveira, A. S.; da Silva, F. M. R.; de Castro Couto, G.; da Silva Boni, M.; Guimarães, M. J. R.; Souza, I. N. O.; Bartolini, M.; Andrisano, V.; et al. Cardanol-Derived AChE Inhibitors: Towards the Development of Dual Binding Derivatives for Alzheimer's Disease. *Eur. J. Med. Chem.* **2016**, *108*, 687–700.

<https://doi.org/10.1016/j.ejmech.2015.12.024>.

(67) Sugano, K.; Hamada, H.; Machida, M.; Ushio, H. High Throughput Prediction of Oral Absorption: Improvement of the Composition of the Lipid Solution Used in Parallel Artificial Membrane Permeation Assay. *J Biomol Screen* **2001**, *6* (3), 189–196.

<https://doi.org/10.1177/108705710100600309>.

(68) Wohnsland, F.; Faller, B. High-Throughput Permeability PH Profile and High-Throughput Alkane/Water Log P with Artificial Membranes. *J. Med. Chem.* **2001**, *44* (6), 923–930. <https://doi.org/10.1021/jm001020e>.

(69) Liu, B.; Wang, L.; Jin, Y.-H. An Effective PSO-Based Memetic Algorithm for Flow Shop Scheduling. *IEEE Trans Syst Man Cybern B Cybern* **2007**, *37* (1), 18–27.

(70) Coghlan, M. P.; Culbert, A. A.; Cross, D. A.; Corcoran, S. L.; Yates, J. W.; Pearce, N. J.; Rausch, O. L.; Murphy, G. J.; Carter, P. S.; Roxbee Cox, L.; et al. Selective Small Molecule Inhibitors of Glycogen Synthase Kinase-3 Modulate Glycogen Metabolism and Gene Transcription. *Chem. Biol.* **2000**, *7* (10), 793–803. [https://doi.org/10.1016/s1074-5521\(00\)00025-9](https://doi.org/10.1016/s1074-5521(00)00025-9).

ABBREVIATIONS

MTDLs Multitarget-directed ligands, MAO monoamine oxidase, GSK-3 β glycogen synthase kinase,

VGCC L-type voltage-gated calcium channels, ChE cholinesterase, hChE human cholinesterase,

hAChE, human acetylcholinesterase, hBuChE human butyrylcholinesterase

For Table of Contents Only

(±)-BIGI-3h: Pentatarget-Directed Ligand combining Cholinesterase, Monoamine Oxidase and Glycogen Synthase Kinase 3 β Inhibition with Calcium Channel Antagonism and antiaggregating properties for Alzheimer's Disease

Lhassane Ismaili*, Julie Monnin, Adeline Etievant, Raquel L. Arribas, Lucía Viejo, Bernard Refouvelet, Ondrej Soukup, Jana Janockova, Vendula Hepnarova, Jan Korabecny, Tomas Kucera, Daniel Jun, Rudolf Andrys, Kamil Musilek, Aurelie Baguet, Eva M García-Frutos, Angela De Simone, Vincenza Andrisano, Manuela Bartolini, Cristóbal de los Ríos, José Marco-Contelles and Emmanuel Haffen

